NON-INVASIVE ELIMINATION OF SUPERFICIAL TUMOURS: A STEP FORWARD

MARIANA MOURA DAS NEVES AMARAL

A dissertation submitted in partial fulfilment of the requirements for the Degree of Masters in Biomedical Research (Specialization Area: Oncobiology)

Dissertação para obtenção do grau de Mestre em Investigação Biomédica (Área de especialização: Oncobiologia)

at Faculdade de Ciências Médicas | NOVA Medical School, NOVA University of Lisbon

October, 2020

NON-INVASIVE ELIMINATION OF SUPERFICIAL TUMOURS: A STEP FORWARD

Mariana Moura das Neves Amaral

Supervisors: Catarina Pinto Reis, PhD, Assistant Professor at Faculdade de Farmácia da Universidade de Lisboa;

and Ricardo A. Afonso, MD, PhD, Assistant Professor at Faculdade de Ciências Médicas | NOVA Medical School, NOVA University of Lisbon

A dissertation submitted in partial fulfilment of the requirements for the Degree of Masters in Biomedical Research (Specialization Area: Oncobiology)

Dissertação para obtenção do grau de Mestre em Investigação Biomédica (Área de especialização: Oncobiologia)

October, 2020

Acknowledgements

Firstly, I would like to thank my supervisors, Professor Catarina Reis and Professor Ricardo Afonso. I am very grateful to Professor Catarina for introducing me to the world of nanotechnology, and for believing in me since the beginning, giving me the freedom to experiment, learn and grow as a researcher and for providing me with all of the opportunities to fuel my growth. I am also very thankful for Professor Ricardo Afonso, for his insightful input throughout the design and execution of the project, and for introducing me to animal models and animal experimentation, and of course for believing in me and in my capacity to grow as a researcher. Although not an official supervisor, I would like to thank Manuela Gaspar for the valuable time that Manuela spent on my project to teach me how to execute different protocols and help with my experiments. I would also like to thank Professor Lia Ascensão, Professor Pedro Faísca, Professor João Pinto Coelho and technician Carla Vânia, for taking their time to help me in the respective techniques and overall contribution to the project. Without you all, this project would never have been possible.

A big thank you to all my colleagues who crossed paths with me at FFUL/iMed.ULisboa, but specially to the ones who I shared every day with, Ana, Joana and Tânia, I am very fund of all the moments we have shared together throughout the year, including lunches, lab mysteries where something disappears, the brainstorming when things went wrong, happy and crazy fun moments, but also the frustrated ones. I am very thankful for all the help you gave me, the double-checking and suggestions of/to my experiments, and I am looking forward to our future years as a team. To my all my friends, but specially to my closest friends, thank you so much for putting up with me every day. To Ana, Raquel, João and Sofia, it would not have been the same without your support. Thank you so much for always listening to me rambling about what goes wrong, for always supporting me in the moments I doubted myself and for not only being there to celebrate our victories but for always being there to cheer me up, I am very grateful to have the bestest friends in the world.

Aos meus Pais, Teresa e Pedro, um grande obrigada por sempre acreditarem em mim e nos meus sonhos, por sempre me incentivarem a segui-los, por me apoiarem e ajudarem com tudo aquilo que podem para que eles se tornem realidade. Vocês são a razão de eu ser quem sou hoje, e nada me dá mais orgulho do que dizer que sou vossa filha. Um grande obrigada também aos meus Irmãos, Pedro e João, que apesar de chatos, me apoiam todos os dias, me ouvem (e fingem que percebem) a falar do meu projeto, e que estão sempre prontos a celebrar as minhas vitórias. Aos meus Avós, que celebram sempre as minhas vitórias, como os artigos científicos em que participo, escritos em inglês que não conseguem ler, um grande obrigada, significa muito para mim ser vossa neta e puder dizer que tenho os avós que tenho. Um obrigado estendido a toda a minha família, incluído primos e tios. Tenho muita sorte em ser da família que sou, e sou muito feliz por isso. Ao Tiago, agradeço toda a paciência, motivação, incentivos e apoio que me dá, por me distrair quando preciso, por me ouvir sempre, por estar sempre pronto a celebrar as minhas vitórias, animar-me quando as coisas correm menos bem, e por me tentar ajudar com tudo o que pode, desde corrigir erros de escrita a escolher figuras, sem ti, eu sei que este percurso não teria sido igual.

Publications

The following publications were partially or entirely used for the preparation of this Dissertation:

- **Mota, A., Sousa, A., Figueira, M., Amaral, M., Sousa, B., Rocha, J., Fattal, E., Almeida, A. & Reis, C., (2020). Natural-based consumer health nanoproducts: medicines, cosmetics, and food supplements. Handbook of Functionalized Nanomaterials for Industrial Applications, 527-578. https://doi.org/10.1016/B978-0-12-816787-8.00019-3**

- **Amaral, M., Afonso, R.A., Gaspar, M.M., & Reis, C.P. (2020). Review article - Anaplastic thyroid cancer: How far can we go? EXCLI Journal, 19, 800-812. https://doi.org/10.17179/excli2020-2257**

Financial Support

The financial support required in order to perform the experimental work for this Dissertation titled “Non-invasive elimination of superficial tumours: a step forward” was provided by *Fundação para a Ciência e a Tecnologia* (FCT) through the Project Reference UID/DTP/04138/2019.

Abstract

Anaplastic thyroid carcinoma is a very rare subtype of thyroid carcinoma and one of the most lethal known malignancies, with a mean survival of 3-5 months. The poor prognosis is mainly due to its undifferentiated nature, inoperability and failing to respond to the typically used therapies for thyroid cancer. Photothermal Therapy (PTT) entails the use of light to increase the temperature of tissues, leading to hyperthermia-mediated cell death. Tumours are more susceptible to the generated heat as they are unable to dissipate it. By using targeted light-absorbing gold nanoparticles (AuNPs), able to transform the light energy into heat, it is possible to target the heat to a specific site, *i.e.,* the tumour.

The aim of this project was to formulate anaplastic thyroid carcinoma-targeted light-absorbing AuNPs able to convert near-infrared light into heat, for PTT applicable to this malignancy.

For this, different cores of AuNPs were synthetized and coated with polymeric material. Particle size, morphology and SPR band were determined. The optimized coated-AuNP core was then functionalized with three ligands to assess anaplastic thyroid carcinoma's specificity. All formulations were tested *in vitro* for safety, efficacy and selectivity. Moreover, the formulations biodistribution and safety profiles were preliminarily assessed *in vivo*.

The different formulations were deemed safe when not irradiated (<30% reduction in cell viability) and selective for anaplastic thyroid carcinoma. Holo-transferrin AuNP was the most cytotoxic when irradiated, promoting 22% of reduction in cell's viability. Regarding the *in vivo* assessments, this formulation was demonstrated as being safe. Taking these all together, this novel formulation seems to be a viable approach for the treatment of anaplastic thyroid carcinoma, to assess in a very near future.

Keywords: Anaplastic Thyroid Carcinoma; Photothermal Therapy; potential innovative therapies; gold nanoparticles.

Resumo

O carcinoma anaplásico da tiroide é um subtipo de cancro da tiróide que, apesar de ser dos mais raros, é um dos mais letais, com uma sobrevida média de 3-5 meses, devido à sua não-diferenciação, fraca resposta a tratamentos e, ao facto de, na sua maioria das vezes, não ser operável. Como alternativa, a terapia fototérmica (PTT) induz morte celular por hipertermia, utilizando energia luminosa como fonte de aquecimento para tecidos. Os tumores são particularmente suscetíveis à hipertermia devido à ineficiente dissipação do calor. Através do uso de nanopartículas de ouro (AuNPs) *direcionadas*, capazes de absorver e converter a energia luminosa em energia térmica, é possível conduzir esta hipertermia a uma localização especifica, como o tumor.

Assim, este projeto teve como objetivo formular AuNPs seletivas para o tratamento de carcinoma anaplásico da tiroide, que absorvam e convertam luz próximo do infra-vermelho, mediando PTT para este tumor.

Neste trabalho foram testados e caracterizados (tamanho, morfologia e banda de absorção) diferentes núcleos de AuNPs. Depois da otimização, as AuNPs foram funcionalizadas com ligandos no intuito de tornar as AuNPs específicas para este tipo de tumor. A segurança, eficácia e toxicidade de cada formulação foram testadas *in vitro*. Foram ainda realizados ensaios *in vivo* de modo a estudar a segurança e biodistribuição das formulações.

Destes estudos, concluiu-se que as AuNPs funcionalizadas revelaram-se seguras (redução de viabilidade celular <30%) e seletivas. As AuNPs funcionalizadas com holo-transferrina foram as que demonstraram maior citotoxicidade para as células cancerígenas sem serem irradiadas, mas também após irradiação com laser, atingindo uma redução na viabilidade celular de 22%. Quanto aos ensaios *in vivo,* foi demonstrada a segurança da formulação.

Considerando os resultados obtidos, esta formulação inovadora sugere ser uma estratégia promissora par o tratamento do carcinoma anaplásico da tiroide, a ser testada num futuro próximo.

Palavras-chave: Carcinoma Anaplásico da Tiróide; Terapia Fototérmica; terapias potencialmente inovadoras; nanopartículas de ouro.

Table of Content

Abbreviations

^{131}I – Radioactive Iodine

Abs – Absorbance

Abs_{max} – Maximum Absorbance Peak

ATA – American Thyroid Association

AuNPs – Gold Nanoparticles

BSA – Bovine Serum Albumin

CT – Computerized Tomography

CTAB – Cetyltrimethil Ammonium Bromide

DMEM – Dulbeco's Modified Eagle's Medium

DMSO – Dimethyl Sulfoxide

EDTA – Ethylenediamine Tetraacetic

EGF – Epidermal Growth Factor

EGFR – Epidermal Growth Factor Receptor

EPR – Enhanced Permeation and Retention

FBS – Foetal Bovine Serum

HA – Hyaluronic Acid

HAOA – Hyaluronic Acid and Oleic Acid

HPLC – High Performance Liquid Chromatography

HTf – Holo-Transferrin

ICP-MS – Inductively Coupled Plasma-Mass Spectrometry

ISO – International Organization for Standardization

Lap – Lapatinib

MRI – Magnetic Resonance Imaging

MTT – Methylthiazolyldiphenyl-tetrazolium Bromide

N/A – Not Applicable

ND – Not Determined

NIR – Near-Infrared

NPs – Nanoparticles

OA – Oleic Acid

OS – Overall Survival

PBS – Phosphate Buffered Saline

PDGFRβ – Platelet-derived Growth Factor Receptor

PdI – Polydispersivity Index

PDT – Photodynamic Therapy

PEG – Polyethylene Glycol

PET – Positron Emission Tomography

PFS – Progression Free Survival

PTT – Photothermal Therapy

RA – Rosmarinic Acid

ROS – Reactive Oxygen Species

RY – Recovery Yield

s.c. – Subcutaneous

SPR – Surface Plasmon Resonances

T_3 – Tri-iodothyronine

T_4 – Tetraiodothyronine

TC – Thyroid Carcinoma

TEM – Transmission Electron Microscopy

Tf – Transferrin

TfR1/CD71 – Type I Receptor for Transferrin

THR – Thyrotropin-releasing Hormone

THST – Thyroid Hormone Therapy

TSH – Thyroid-stimulating Hormone

TSHR – Thyroid-stimulating Hormone Receptor

UV – Ultraviolet

VEGFR – Vascular Endothelium Growth Factor Receptor

List of Figures

List of Tables

1. Introduction

1.1 Nanotechonolgy, Nanomedine and Nanoparticles[1]

Nanotechnology has become an excellent platform with many applications in different fields of science, allowing to control and manipulate matter at the nanoscale by designing and engineering new systems [1,2]. The application of nanotechnology for medical purposes is called nanomedicine. This exponentially-growing field is expected to significantly impact the quality of health care through the improvement of diagnostic tools, prevention and treatment of many diseases [3,4]. Nanomedicine could potentially provide improved and cost-effective healthcare, allowing availability and affordability [5]. In fact, the nanomedicine industry market value is expected to reach a total of US$334 billion by the end of 2025 [6]. Converting a material into the nanoscale has many advantages, including very high surface area-to-volume ratio, precise drug delivery, modification of transport mechanism through biological barriers and different alterations in the physicochemical properties of the material by itself [5,7]. Moreover, as many biological processes occur at the nanoscale, and as nanomedicine allows to cross biological barriers, it can provide novel opportunities to interact with such processes, which is important for both imaging and drug delivery [5].

Nanomedicine-based therapeutics have contributed to the development of innovative treatment approaches of different nature (*i.e.,* antitumoral, antiviral, anti-inflammatory) [8], particularly relevant when applied to cancer treatment [9]. Many NPs-based products have been approved for the treatment of various tumors, some of them still in various phases of clinical trials [10]. Approved by the FDA (1995) and the EMA (1996), Doxil® was the first liposomal-encapsulated doxorubicin formulation. This anticancer drug showed superior clinical performance in a variety of neoplasms due to its pharmacokinetics and biodistribution, having reduced adverse side effects and improved overall patient compliance and quality of life [11]. This formulation contains PEG chains on the liposomal surface. This characteristic increases the longevity of the liposomes in the circulation system [12]. Moreover, DaunoXome® is a liposomal formulations of daunorubicin, used for the treatment of different solid malignancies, including AIDS-related Kaposi's sarcoma, breast cancer and ovarian cancer; and Abraxane®, a nanoencapsulated paclitaxel using albumin-based

[1] Section *1.1 Nanotechonolgy, Nanomedine and Nanoparticles* is adapted from the following publication by our group (with permission of the copyright holder): **Mota, A., Sousa, A., Figueira, M., Amaral, M., Sousa, B., Rocha, J., Fattal, E., Almeida, A. & Reis, C., (2020). Natural-based consumer health nanoproducts: medicines, cosmetics, and food supplements. Handbook of Functionalized Nanomaterials for Industrial Applications, 527-578. https://doi.org/10.1016/B978-0-12-816787-8.00019-3**

nanoparticles directed to breast and lung cancers [9,13]. These formulations improved the quality of life of patients treated with the nanoencapsulated drugs by diminishing the adverse side effects associated with such drugs.

Different nanosystems applied to cancer treatment and/or diagnosis include: liposomes, nanoparticles (NPs), dendrimers, polymeric micelles, nanocantileveres, carbon nanotubes and quantum dots [9]. NPs are described as being molecular assemblies of functional chemicals and molecules, and can differ not only in the materials in its' constitution, as well as its' size (1-1000 nm) and other physicochemical properties [14,15]. As mentioned, NPs can be made from different materials, and according to the used material, NPs are categorized as: organic NPs, usually lipid-, carbon- or polymeric-based; or as inorganic NPs, made from materials such as metals [16]. The main application of these nanosystems in cancer treatment are mainly as targeted-drug delivery systems as these elicit enhanced drug bioavailability and delivery to the desired site. Therefore, NP-delivered drugs lead to higher drug concentration in the targeted site, through one of two forms of targeting: active targeting and passive targeting [17,18]. Active targeting consists on modifying the nanosystems' surface with a targeting moiety, usually an antibody for a specific biomarker present in the cancer cell or a ligand for an overexpressed receptor. Besides enabling targeted delivery of a drug, active targeting can also promote faster internalization of the NP by the targeted cancer cell, through receptor-mediated endocytosis [17,19]. On the other end, passive targeting requires the understanding of the enhanced permeation and retention (EPR) effect, resulting from the enhanced permeability of the incomplete tumour blood vessels and the enhanced retention originated from lack of tumoral lymphatic drainage [19,20]. The tumour's microenvironment is deeply vascularized due to the abnormal secretion of different pro-angiogenesis factors [21]. The blood vessels present in the tumours' microenvironment have enhanced permeability due to faulty angiogenesis, originating blood vessels with open inter-endothelial junctions or open transendothelial channels [20]. The presence of such gaps in tumoral blood vessels, with a size cut-off of about 400 to 1000 nm, much bigger than the normal gaps between endothelial cells (5 to 10 nm), allows NPs that were circulating in the blood system to extravasate into the tumour interstitium [19]. Due to incomplete and inefficient lymphatic vessels, NPs are not rapidly cleared from the interstitium, and thus are retained in the tumour [17,20]. Therefore, passive targeting takes advantage of the normal biodistribution of the NPs into the tumour, as well as of the EPR effect [19].

1.2 Gold Nanoparticles (AuNPs) and Photothermal Therapy (PTT)

Historically, gold has been used in medicine to treat diseases affecting mainly the skin (*i.e.,* smallpox, measles and skin ulcers) by ancient civilizations from Egypt, India and China (*e.g.*), and is currently used for the development of medical devices to treat cardiovascular diseases and earing problems, for example [18]. Gold nanoparticles (AuNPs) are a type of inert inorganic NPs with interesting applications in nanomedicine due to its unique and versatile optical and physicochemical properties, biocompatibility, stability and low cytotoxicity [22]. These applications include a variety of fields, such as biosensors, diagnostics, vaccines, molecular imaging, drug delivery and theranostics [18,23,24]. When applied to cancer diagnosis, AuNPs can improve tumour computerized imaging (CT scan), by labelling cancer cells, due to its property to absorb much more X-ray radiation than any soft tissue and can also be used as probes for near-infrared (NIR)-imaging of tumour cells [25]. Furthermore, AuNPs can be functionalized or carry imaging and/or radiosensitive agents in order to improve the already established tools for cancer imaging (*i.e.,* positron emission tomography - PET, CT scan, magnetic resonance imaging - MRI) [18,25]. Employing AuNPs, instead of other nanosystems, for better imaging of tumours has advantages, such as higher biocompatibility, as well as better and a more controlled colorimetric contrast, due to their optical properties, which vary according to size, shape and surface functionalization [18]. Regarding cancer therapeutics specifically, AuNPs have shown to present a broad variety of potential applications and have been studied for drug delivery (chemotherapy), radiotherapy, immunotherapy, photodynamic therapy (PDT) and photothermal therapy (PTT) [18,24,26–29]. AuNPs have been tested as possible drug delivery systems for different chemotherapy agents, such as platinum derivates (*i.e.,* cisplatin, carboplatin and oxaliplatin) and anthracyclines (*i.e.,* doxorubicin and epirubicin), as well as delivery systems of cancer antigens and immune adjuvants, enhancing cancer immunotherapy [26,30–33]. Furthermore, AuNPs have also been applied to radiotherapy as radiosensitizers to physical and chemically enhance the ionizing radiation dose and to improve the chemical sensitization of DNA to the ionizing radiation emitted [34]. Moreover, AuNPs can improve the targeting of the radiation to the tumour, reducing the damage to the surrounding tissues, and further enhancing the therapeutic effect through increasing the production of free radicals and other reactive species [27].

PDT and PTT are phototherapies that entail the use of light to ablate localized tumour masses, but through different mechanisms, as depicted in Figure 1[35,36].

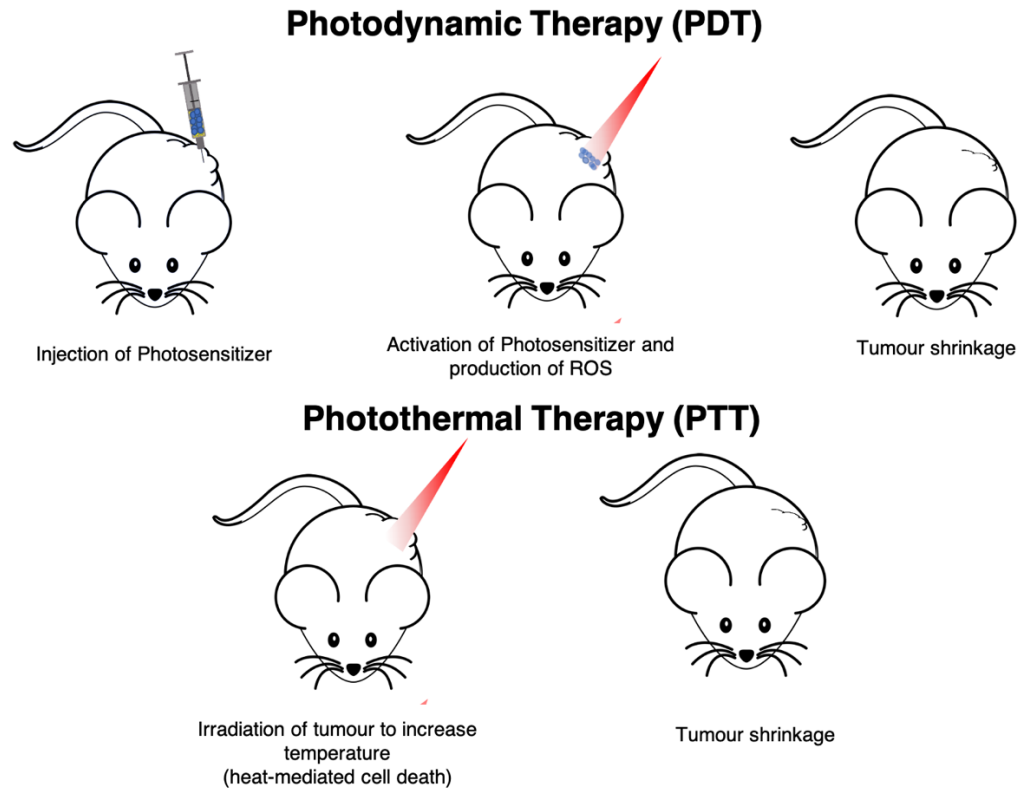

Figure 1. Main differences between photodynamic therapy (PDT) and photothermal therapy (PTT) mechanisms of action in tumour shrinkage.

PDT uses photochemical reactions produced through the photoactivation of photosensitizer drugs, when irradiated with the adequate wavelength, originating reactive oxygen species (ROS) [37,38], which promote cell death. AuNPs are usually used in PDT with the main purposes of improving the delivery, targeting and accumulation of photosensitizers drugs to/in tumours, through incorporating the photosensitizer into the AuNPs or/and by conjugating to the surface of AuNPs [37,39,40].

In contrast, PTT does not use photosensitizers nor photochemical reactions, taking advantage of a different mechanism of action. PTT uses light/heat sources, such as visible light, radiofrequency waves, microwaves, ultrasound waves, ultraviolet (UV) and NIR light, in order to increase the local temperature and ablate the tumour mass by hyperthermia [36]. The hyperthermia generated at the tumour site causes the cancer cells to undergo irreversible damage, usually characterized by protein denaturation and disruption of the cellular membranes, culminating in hyperthermia-mediated cell death [37,41,42]. In comparison to the current commonly therapies used to treat cancer, PTT presents many advantages such as

minimal invasiveness, low toxicity and spatial-temporal specificity [41,43]. Furthermore, PTT presents a high specificity to neoplastic tissues or tumour cell masses, since these present an incomplete vasculature, which unables them to dissipate the heat generated from the light source through their blood vessels and therefore tend to reach higher temperatures, making them more prone to heat-mediated cell death [42]. Although hyperthermia-based treatments have been used for many years, there are still some limitations associated to PTT-based cancer treatments [44,45]. The main limitation relates with the difficulty to induce homogeneous and precisely-localized hyperthermia without resorting to more invasive approaches (*i.e.,* inserting antennas to the local of the tumour). Another important problem related with the use of PTT results from the poor penetrating capacity of the radiation used, since human tissues present high extinction coefficients, therefore limiting PTT-based treatments to superficial and localized tumours [45].

Applying combined PTT and nanotechnology approaches can overcome the above-mentioned limitations to PTT. Indeed, using photoabsorbent NPs, one can change the photothermal properties of the medium and therefore enhance the hyperthermic effect on tumours [46]. In order to enhance PTT efficacy, NPs are required to present the following set of characteristics: high absorbance at the wavelengths of biological windows (700-980 nm and 1000-1400 nm), since intervals tissues' scattering and absorption is reduced at these wavelengths, allowing radiation to reach the tumour site in order to achieve maximum absorption and conversion into thermal energy by the NPs. It has been described that NPs generally present also low toxicity when not activated by laser, ensuring that no tissues are harmed before the NPs reach the desired site [45]. Also, NPs allow easy surface functionalization and therefore provide higher selectivity of the PTT-generated hyperthermia to the cancerous mass [45].

NPs with applications in PTT can be made of different materials, with a special focus in inorganic metal-based NPs, including iron oxide-based NPs, palladium-based NPs, copper-based NPs and AuNPs [47,48]. In addition to inorganic NPs, NPs for PTT can also be developed from organic materials, examples of such including carbon-based NPs (*e.g.,* graphene NPs, carbon dots and carbon nanotubes), micelles, liposomes and protein/polymer-based NPs [48,49]. Gold-based NPs, made entirely or partially of gold, have many advantages when used in NP-based PTT, compared to other NPs [50]. Such advantages include efficient light-heat conversion and tunnable optical properties that can be manipulated through varying the AuNPs physical characteristics, such as size and shape [18,50,51]. AuNPs are considered plasmonic NPs, as their characteristic optical properties are a result of the surface plasmon

resonances (SPR) phenomenon [51,52]. In this phenomenon, free electrons present at the interface between the metallic surface and the adjacent medium oscillate in resonance with external electromagnetic fields generated by the light sources, resulting in charge separations and consequent dipole oscillations [51,52]. These resulting oscillations are amplified at the SPR frequency, causing high degree absorption of the photons emitted by the light source at the SPR wavelengths [51,52]. The SPR wavelengths of AuNPs can be manipulated through modifying its' composition, size, structure and shape [52]. The majority of the AuNPs synthetized for PTT applications present SPR bands at wavelengths bellow the biological window, in the UV or visible spectrum, which present poor penetration into human tissues and thus are suitable for the treatment of very superficial tumours only, such as skin cancers [53–55]. Moreover, AuNPs can also be designed to absorb in the NIR range of the light spectrum (650-950 nm), allowing the treatment of more internal solid tumours, localized up to 2-3 cm bellow the skin [56,57].

There have been many advances regarding the use of AuNP-mediated PTT with NIR light to treat solid tumours and NIR-activated AuNPs have been proposed for the treatment of many cancers, including melanoma [58,59], lung cancer [60], breast cancer [61], prostate cancer [62], liver cancer [63] and colon cancer [64]. Some of the cited examples mention functionalized AuNPs, with ligands such as epidermal growth factor (EGF) [58] and anti-EGF receptor (EGFR) antibodies [60,61], which allow, through active targeting, to improve tumour targeting and formulation specificity, avoiding accumulation of AuNPs in off-target organs, and therefore with substantial decrease of the side effects. AuNPs allow functionalization with a large variety of ligands through an array of processes, such as: covalent conjugation, normally associated with the conjugation of biomolecules (*i.e.,* DNA, proteins, peptides, some drugs) and the establishment of gold-thiol chemistry, allowing the ligand to attach to the AuNPs' surface through secondary tethering; and non-covalent conjugation, that occurs by processes such as specific binding affinity, electrostatic or by hydrophilic interactions [57,65,66].

There are some concerns regarding the long-term toxicity of NPs, in general, mainly driven by using toxic chemicals to synthetize these systems and ineffective clearance of NPs from its' accumulation sites [57]. Such concerns can be addressed by modifying the NP surface through ligand conjugation, or for example by adding an external coating [57]. Examples of commonly used coatings for AuNPs are the addition of polyethylene glycol (PEG) [62] and other polymers [67,68], chitosan [63], protein-based coatings (*i.e.,* bovine serum albumin, BSA) [69], amorphous silica [70,71] and lipids [72].

1.3 Anaplastic Thyroid Carcinoma [2]

Thyroid is a butterfly-shaped gland composed by two lobes, located medially in front of the neck, below the larynx and posteriorly to the tracheal thyroid cartilage [73]. This gland has a functional unit, the thyroid follicle, a cystic structure composed of a single layer of follicular cells [74]. These units store thyroglobulin, involved in the synthesis of thyroid hormones (*i.e.,* tri-iodothyronine, T_3; and tetraiodothyronine, T_4) [74,75]. Thyroid hormone production and secretion are controlled by the hypothalamus-pituitary axis, comprising the release of thyrotropin-releasing hormone (TRH) from the hypothalamus, and thyroid-stimulating hormone (TSH), from the pituitary [74,76]. Upon release by the pituitary, TSH binds to the TSH receptor (TSHR) of the follicular cells' membrane, stimulating the synthesis and release of the thyroid hormones [74,76]. Regulation of thyroid function is achieved almost entirely by a negative feedback mechanism carried out by T_3 and T_4 on hypothalamus and pituitary.

T_3 and T_4 are known to play important roles in the human body, such as promoting the growth and differentiation of many tissues, as well as energy and metabolic homeostasis, due to their involvement in different metabolic pathways [77]. Moreover, the thyroid gland also comprises neural-crest derived parafollicular C-cells, located in-between thyroid follicles and responsible for calcitonin secretion [78], which promotes calcium and phosphate renal elimination and deposition in different tissues [78].

Although thyroid cancers account for only 2.1 % of all cancers diagnosed worldwide, it is one of the most frequent endocrine malignancies [79–81]. As with other malignancies, thyroid cancers differ in their morphology, invasiveness and molecular profile [81,82].

Taking into account their histopathology, thyroid carcinomas can be classified as well-differentiated (medullary, papillary and follicular thyroid carcinoma) or undifferentiated (anaplastic thyroid carcinoma) [82–84], as summarized in Table 1.

[2] Section *1.3 Anaplastic Thyroid Carcinoma* is adapted from the following publication by our group (with permission of the copyright holder): **Amaral, M., Afonso, R.A., Gaspar, M.M., & Reis, C.P. (2020). Review article - Anaplastic thyroid cancer: How far can we go?. EXCLI Journal, 19, 800-812. https://doi.org/10.17179/excli2020-2257**

Table 1. Classification of thyroid carcinomas (TC).

Cell Type	Subtype	
Unknown	Anaplastic TC	Undifferentiated
Follicular	Papillary TC Follicular TC	Well-Differentiated
Parafollicular C-cells	Medullary TC	

1.3.1 Epidemiology and Prognosis

Papillary thyroid carcinoma accounts for the largest portion of thyroid carcinomas (70-80%), being the least aggressive due to slowly-forming metastasis and low invasiveness [85]. Follicular thyroid carcinoma is a more aggressive subtype of well-differentiated thyroid carcinoma, due to its usual later diagnosis, and accounts for 10% of thyroid malignancies [86]. Medullary thyroid carcinoma accounts for 5-10% of thyroid malignancies, originates from parafollicular C-cells, is associated with a mutation of the *RET* proto-oncogene and can be sporadic or familial (25% of medullary thyroid carcinomas) [87]. Another form of hereditary thyroid carcinoma is familial non-medullary thyroid carcinoma, englobing all hereditary thyroid carcinomas originating from thyroid follicular cells [88,89]. Although familial non-medullary thyroid carcinoma is inherited through an autosomal dominant pattern, the associated mutated genes are not yet identified [89].

Anaplastic thyroid carcinoma is a form of undifferentiated thyroid carcinoma, which although rare (<2%), is one of the most lethal malignancies, being characterized by high aggressiveness, due to both fast growth and strong invasiveness, as well as low responsiveness to most therapies currently available [90,91]. Moreover, although anaplastic thyroid carcinoma arises from thyroid follicular cells, these cells loose its thyroid-like features, leading to very poor prognosis [92]. The overall 5-year survival rate upon anaplastic thyroid carcinoma diagnosis is lower than 10%, and most patients do not live longer than a few months after diagnosis [93].

These two groups of malignancies have different aggressiveness. Indeed, well-differentiated thyroid carcinomas are known to be more manageable, with higher survival rates, whereas undifferentiated thyroid carcinomas are known to be more aggressive, with higher invasiveness and poorer prognosis, normally non-operable and having poor treatment response rates [94]. Well-differentiated thyroid carcinomas include malignancies derived from the thyroids' follicular cells, such as papillary and follicular thyroid carcinomas [95]. Anaplastic thyroid carcinoma is an undifferentiated subtype with very poor survival

prognosis, estimated to be 3 to 5 months after diagnosis, and survival rates of 10-20% and less than 5% after 1 and 10 years, respectively [96]. Although this rare tumor has an incidence of only 1-2 persons per million per year, it is responsible for 40% of all thyroid cancer deaths [97,98]. The very poor prognosis is associated to anaplastic thyroid carcinoma only being detectable by the current diagnostic tools at advanced stages and, furthermore, being unresponsive to the current treatments available [82].

In similarity to what is seen for malignancies of other tissues and/or organs, there are risk factors associated with the increased chances of developing thyroid carcinomas. Such risk factors include radiation exposure to the chest or neck area, abnormal iodine intake leading to iodine deficits, previously-existing thyroid pathologies (*i.e.,* goiter and Hashimoto's Thyroiditis) and metabolic disorders (*i.e.,* diabetes and obesity) [99]. There are some etiologic factors specifically associated with the development of anaplastic thyroid carcinoma, both as primary disease or by dedifferentiation of other thyroid malignancies. Such etiological factors include irradiation and abnormal TSH levels [100]. The biggest risk factor for developing this rare undifferentiated carcinoma seems to be prior history of goiter, both of self and familial [96]. Furthermore, risk factors generally include previous history of other thyroid malignancies, as these can give rise to anaplastic thyroid carcinoma through dedifferentiation [100,101]. Anaplastic thyroid carcinoma seems to occur most frequently in the elderly, being diagnosed at around 65-72 years old [102]. Generally, both well-differentiated and anaplastic thyroid carcinoma affect women 2 to 3 times more than men [103].

1.3.2 Pathophysiology and Histology

As previously mentioned, based on their histology and behavior, thyroid carcinomas can be subcategorized in well-differentiated and undifferentiated (anaplastic) thyroid carcinomas. Regarding histology, well-differentiated thyroid carcinoma arises from the thyroids' follicular cells and can be classified as papillary, if a papillary pattern is seen, or follicular, if a follicular pattern is found [104]. Although both patterns may be present, classification is based on the most prevalent pattern observed [104]. Furthermore, well-differentiated thyroid carcinoma aggressiveness is determined by assessing the presence of capsular and/or blood vessels invasion [105]. Usually, papillary thyroid carcinomas present as an encapsulated mass, not invasive, whereas the follicular subtype presents high invasiveness, of both capsule and blood vessels. Papillary thyroid carcinomas can be further distinguished into two classes

according to molecular profiling: *BRAF*-predominant; and *RAS*-predominant, the last associated with increased aggressiveness [105].

Usually, thyroid carcinoma staging is determined by age, histology, size, extra-glandular invasion and presence of distance metastasis [106]. Regardless of the patient's and tumor status based on the mentioned characteristics, anaplastic thyroid carcinomas are always classified as stage IV [85,90,107]. Then, by assessing different parameters, it can be sub-classified as: stage IVA, if it is confined to the thyroid; stage IVB, when there is extra thyroidal disease; or stage IVC, once distant metastasis are present [108].

Anaplastic thyroid carcinoma is often clinically characterized as a large palpable rapidly growing mass, causing symptoms such as hoarseness, dysphagia, dyspnea, and in advanced cases, superior vena cava syndrome and Horner's syndrome [109,110]. Histologically, the characteristic cells of this tumor are known to have undergone epithelial-mesenchymal cell phenotype transition [82]. Furthermore, histological findings may follow one of three patterns according to the main cellular population present being giant, spindle or squamous cells [109,110]. This leads to uncertainty of the organ of origin, culminating in delays in diagnostic and in initiation of treatment [109,110]. Although these histological differences may be present, they do not significantly influence prognosis [111]. Macroscopically, regardless of its cellular heterogeneity, anaplastic thyroid carcinoma presents characteristically as large light tan color tumors, with marked invasiveness and mitotic activity, high proliferation, presence of hemorrhage and large areas of necrotic tissue, but decreased apoptosis [111].

Although this undifferentiated malignancy can arise primarily, there is clinical, pathologic and epidemiologic evidences supporting that it can originate from the dedifferentiation of previously-existing well-differentiated thyroid carcinomas [112,113]. Such evidence includes the fact that these tumors can coexist and that some treated well-differentiated thyroid carcinomas relapse as anaplastic thyroid carcinomas [114]. Furthermore, the genetic modifications and oncogenes that give rise to follicular and/or papillary thyroid carcinomas are also observed in anaplastic thyroid carcinomas [112,113,115]. Moreover, anaplastic thyroid carcinoma harbors some characteristic genetic features [116]. For example, gain of function mutations of the *PIK3CA* gene are frequently seen in anaplastic thyroid carcinoma, but not in well-differentiated thyroid carcinomas [116]. Mutations in the gene encoding β-Catenin, *CTNNB1*, are commonly associated with epithelial-mesenchymal transition, which has been speculated as being one of the main processes behind this malignancy pathogenesis [94,116]. The previously mentioned mutations are gain of function of important oncogenes, but the loss of function and inactivation of tumor suppressor genes are also present in

anaplastic thyroid carcinoma [116,117]. Such genes include *p53* and *PTEN*, both negative regulators of proliferation and inducers of apoptosis [94,117,118]. Thus, the inactivity of these genes lead to increased aggressiveness, and are present in this non-differentiated tumor [116]. Anaplastic thyroid carcinoma shares mutations with follicular and/ or papillary thyroid carcinomas, such as point mutations in *BRAF* and *RAS*, but these mutations are more common in the differentiated subtypes [116,117,119]. Furthermore, the overexpression of receptors, such as EGFR, are not only characteristic of anaplastic thyroid carcinoma but also of thyroid and primary thyroid carcinomas dedifferentiation or anaplastic carcinoma transformation [120,121].

Like other cancers, anaplastic thyroid carcinoma presents altered expression (*i.e.,* overexpression, low expression or loss of expression) of many receptors when compared to healthy thyroid tissues, and have been hypothesized as being contributors to tumour genesis and disease progression, including growth factor receptors such as HER-2, platelet-derived growth factor receptor (PDGFRβ), vascular endothelium growth factor receptor (VEGFR) and EGFR, as already mentioned [122–124]. EGFR is a family of transmembrane growth-factor receptors tyrosine kinases overexpressed in anaplastic thyroid carcinoma (EGFR/ErbB-1, HER2/ErbB-2, HER3/ErbB-3 and HER4/ErbB-4) that take part in a complex signalling cascade that mediates many cellular processes, including cell proliferation, survival, adhesion, migration and differentiation [125,126]. Aberrant activation of EGFR, through its' overexpression or overactivation of normally-expressed EGFR, in cancer cells leads to an increase of the cells' capacity to grow and survive, mediating tumorigenesis and dedifferentiation, increasing the tumour aggressiveness [127,128]. The role of EGFR in thyroid cancer progression has been described as being mediated through the overactivation of the MAPK and PI3K/AKT signalling pathways, that regulate cell growth, proliferation, cell death through apoptosis, and metabolic processes, both through the gene expression regulation [129,130].

Moreover and in similarity to other malignancies, anaplastic thyroid carcinoma also presents overexpression of the type II cell membranase-associated glycoprotein, type I receptor for transferrin (TfR1/CD71), responsible for transferrin (Tf)-mediated iron import and mainly involved in iron homeostasis and cell growth when in physiological conditions [131,132]. This ubiquitously expressed receptor is expressed in healthy thyroid tissues, but have low levels of membrane incorporation, when in physiological conditions, acquiring an aberrant expression profile during tumorigenesis and tumour progression [131]. Abnormally

expressed TfR1/CD71 is involved in different key processes in cancer, such as promoting cancer cells' proliferation, migration, invasion, apoptosis and metastasis [132].

1.3.3 Diagnosis

Well-differentiated thyroid carcinomas, such as follicular or papillary thyroid carcinomas, are usually asymptomatic and are diagnosed upon physical and/or ultrasonography examination [133]. In rare occasions, well-differentiated thyroid carcinomas may present symptoms such as a palpable and growing neck mass, hoarseness, dysphagia and/or with cervical lymph-node metastases [133].

Anaplastic thyroid carcinoma generally presents more serious symptoms, including hoarseness, airway distress, dyspnea and dysphagia, caused by a fast growing neck mass [134,135].

In order to classify a thyroid nodule as malignant or benign, TSH serum levels are evaluated, and a combination of histological, cytological and imaging techniques are used. TSH serum levels allow to differentiate between hyperfunctioning and non-functioning nodules [85]. Thyroid carcinomas often present non-functioning thyroid nodules, and thus, other tests are generally required [85].

Definitive diagnostic is usually achieved by fine-needle aspiration biopsy and/or high-resolution ultrasonography [85,136,137]. Papillary, medullary and anaplastic thyroid carcinomas are diagnosed according to the results of these examinations, but additional histological tests can be necessary to differentiate between follicular thyroid carcinoma and benign follicular thyroid adenomas [138].

1.3.4 Current Treatment Approaches

Currently, thyroid cancer is treated by using a combination of radioactive iodine therapy, thyroid hormone suppression therapy and surgery. Nevertheless, the chosen treatment is defined according to different factors, such as the subtype of cancer and stage of disease [85].

Total or partial surgical resection of the thyroid gland remains one of the first options for both well-differentiated and undifferentiated thyroid carcinomas, although in the latter total thyroidectomy is unusual due to invasiveness of the disease [109,139].

Therapy with radioactive iodine has been used to treat thyroid cancer since 1946 [140]. For radioactive iodine therapy to be effective, a high level of thyroid-stimulating hormone (TSH or thyrotropin) must be present in the blood to promote its uptake/or absorption. To

synthetize thyroid hormones, the thyroid follicular cells need to uptake iodine, a substrate required for the synthesis of these hormones. Iodine is internalized by the follicular cells through iodine symporter channels. Inside the follicular cells, the iodine is oxidized and bound to tyrosyl residues of thyroglobulin, giving rise to tri-iodothyronine (T_3) and tetraiodothyronine (T_4), with three and four atoms of iodine, respectively [141,142]. When in the presence of Radioactive Iodine (^{131}I) instead of normal iodine, the ^{131}I undergoes the previously described processes in the follicular cells, leading to tissue necrosis mediated by its beta emissions. As a result, this necrosis will lead to the ablation of the functional tissues of the thyroid gland [142,143]. Conventionally, this therapy is used after surgery, either as an adjuvant therapy or to treat any tumoral residual tissue [144,145]. Undifferentiated and medullary thyroid carcinomas do not respond to this therapy as they are characterized by a lack of expression of thyroid cell markers and behavior, being unable to uptake iodine and consequently produce T_3 and T_4 [109,138].

Usually, life-long thyroid hormone therapy (THST) is used to treat well-differentiated and medullary thyroid carcinomas after thyroidectomy and radioactive iodine therapy to prevent thyroid-stimulating hormone (TSH)-dependent proliferation of any residual well-differentiated thyroid cancer cells [138,146,147]. Physiologically, TSH release by the pituitary is inhibited by high serum levels of T_3 and T_4, *i.e.,* through a negative feedback mechanism [141]. Thus, this therapy involves the administration of T_3 and T_4, increasing serum levels of these two hormones and inhibiting pituitary TSH release [141]. Moreover, besides inhibiting TSH-dependent proliferation of cancer cells, THST also corrects the surgically-induced hypothyroidism of patients who undergo total or partial thyroid resection [141].

Medullary thyroid carcinomas and undifferentiated thyroid carcinomas are usually unresponsive to the conventional course of therapy used for well-differentiated thyroid carcinomas: radioactive iodine therapy, THST and surgery [148]. For this reason, systemic chemotherapy is used for the treatment of the mentioned malignancies, and also for the treatment of non-resectable, radioactive- iodine-non-responsive, recurrent or metastatic, well-differentiated thyroid carcinomas [148,149].

a) Treatment of well-differentiated thyroid carcinomas

Currently, well-differentiated (papillary and follicular) thyroid carcinomas are treated by using a combination of surgery to remove the thyroid and, if necessary, radioactive iodine

therapy and THST. It has been reported that patients with stage II or well-differentiated high-risk thyroid carcinoma benefit from radioactive iodine therapy, improving their overall survival [144]. This is not the case for patients with stage I well-differentiated thyroid carcinomas, whose overall survival worsens when ^{131}I is used [144]. Furthermore, radioactive iodine therapy can also be useful for patients with metastatic disease, in which the distant neoplastic *foci* have thyroid-like features, responding to treatment and ^{131}I uptake [109]. Thus, although radioactive iodine therapy is efficient in many cases, it has severe side effects associated to it such as off-target organ damage (*i.e.,* salivary glands and bone marrow) and increasing the patients risk of developing hematologic malignancies [150].

Furthermore, THST has been shown to be an efficient therapy for the treatment of well-differentiated thyroid carcinomas, increasing the patients' overall survival, reducing disease recurrence and cancer-related mortality [109,144]. Moreover, high-risk well-differentiated thyroid carcinoma patients strongly benefit from this therapy, whose survival can be increased 2 to 3 fold-factor [138].

In the case of metastatic and/or advanced well-differentiated thyroid carcinomas, systemic chemotherapies are used. But, unfortunately, these malignancies are associated with poor response rates and short time of response when systemic therapies are used [151]. Some of the cytotoxic drugs used for the treatment of advanced thyroid carcinoma include doxorubicin, paclitaxel, tamoxifen, bleomycin, epirubicin, cisplatin and octreotide [148,151–153]. The choice of systemic therapies is somewhat inconclusive, as reports with different response rates to the same protocols are observed. For example, doxorubicin, the most studied and used chemotherapy agent for these malignancies, seems to be one of the cytotoxic drugs with the highest response rate, ~40%; but this response is temporary and most responses to this drug are incomplete [138]. Other studies show that some patients only have a response rate of ~17%, for the single use of doxorubicin, displaying however, an increase in response rates when combined with cisplatin or even achieving complete responses [154,155]. Altogether, doxorubicin seems to be the most effective in treating metastatic disease, that are non-responsive to other treatments, as well as for medullary thyroid carcinoma, either as a single-agent chemotherapy or in combination with other agents [153]. Such combined regimens include: doxorubicin, bleomycin and vincristine; or bleomycin, doxorubicin and cisplatin [153].

When administered at low doses, cytotoxic agents can be used as radiosensitizers for external radiation therapy to increase its efficacy [154].

b) Treatment of Anaplastic Thyroid Carcinoma

According to the most recent American Thyroid Association (ATA) guidelines, to manage and control local and metastatic anaplastic thyroid carcinoma, a combination of surgery, chemotherapy and radiotherapy should be used [156]. Surgery for local disease management should be applied when total or major part of the mass is resectable, without damaging the surrounding vital structures (*i.e.,* trachea, larynx, vocal cords, esophagus, major vessels and nerves, etc.). ATA also describes that only a small percentage of patients fit these criteria. In palliative care, surgery can improve quality of life, for example by decompressing the patient's airway. Regardless of potential-curative or palliative intent of treatment, tracheostomy is recommended by ATA for airway management [108]. As adjuvant or primary course of treatment, radio- and chemotherapy are also used. Different cytotoxic drugs are used, such as regimens combining paclitaxel and carboplatin, or docetaxel and doxorubicin, but multimodal chemotherapy regimens composed of only one cytostatic drug, such as cisplatin, paclitaxel and doxorubicin, are also part of the therapeutic options. In the case of advanced metastatic disease, surgery and radiotherapy are not recommended, being the systemic therapies the most appropriate.

For this, anthracyclines and platins are used as first-line cytotoxic chemotherapy regimens. Overall survival seems to be maximized when the three presented therapeutic options are combined [157].

Although the above-described therapeutic options are available, both individually and combined, its efficacy in treating and curing patients with anaplastic thyroid carcinoma is very low [157]. For example, although it has been described that total resection of tumor increases 1 year survival to 92%, the mean survival of patients that undergo surgery is 3.5 months [158]. Radiotherapy alone does not seem to improve survival (2.3 months), but in combination with surgery and chemotherapy, survival rates of 2 years after diagnosis, for some patients, are reported [96,158].

Radiotherapy has no effect in disease re-occurrence, with half of the patients relapsing when treated with radiotherapy alone [158]. Due to the recurrence rate, cytotoxic agents such as doxorubicin, can also be used as radiosensitizers, improving local long-term control rate (68 %). Although this cytotoxic agent is the most used in chemotherapy regimens for anaplastic thyroid carcinoma, its response rate is around 22% [96,157,158]. Paclitaxel and docetaxel, also used in chemotherapy regimens, show a response rate of around 53 and 14%, respectively [96,157]. Regimens composed of only cisplatin, bleomycin and methotrexate also have poor response rates [96]. The poor response rates presented might be due to

anaplastic thyroid carcinoma expressing multidrug resistance-associated proteins and due to the presence of cancer stem cells [96,159]. Although systemic treatment with chemotherapy has achieved promising results, combining doxorubicin and cisplatin seems to be more effective in reducing mass size, being, for this reason, the standard systemic therapeutic regimen [157,158].

c) Novel therapies

To overcome the lack of both efficacy and tumor selectivity, nanosystems-based therapeutic approaches have been developed with promising results. One example is the copper-based nanosystems for radiotherapy and Photothermal Therapy (PTT), used to treat thyroid carcinomas [160]. PTT is a non-pharmacologic and less invasive approach to target and reduce tumors by thermal ablation of cancer cells, with minimal side effects when compared to other therapeutic options [161], as represented in Figure 2. A gold-based nano hybrid approach has been developed for the treatment of melanoma, also showing very promising results for the treatment of other tumors, such as anaplastic thyroid carcinoma [58,161].

Moreover, an incoming therapeutic approach for the treatment of anaplastic thyroid carcinoma is using targeted inhibitors for hyperactive and/or mutant components of signaling pathways [162]. As previously mentioned, members of the RAF/ MAPK and MEK pathway are mutated in this malignancy (*i.e.,* EGFR, *BRAF*, *Ras*) [114,162,163]. Recent studies reported promising results, either of decrease in tumor mass or good responses, using targeted/multi-targeted therapies, both individually or combined, enlightening the benefits of using sequencing tools to identify possible targets for each patient [98]. Furthermore, small-molecule tyrosine kinase inhibitors, such as sorafenib [96], vemurafenib [164], dabrafenib [165], and trametinib [165], have been shown to be promising for the treatment of anaplastic thyroid carcinoma, being currently in clinical trials, alone or in combination (*i.e.,* dabrafenib + trametinib) [96,98,165]. However, when a small-molecule tyrosine kinase inhibitor was used alone, disease reoccurrence was reported by most patients [162]. Table 2 summarizes the promising results of completed clinical trials using small-molecule tyrosine kinase inhibitors for the treatment of anaplastic thyroid carcinoma.

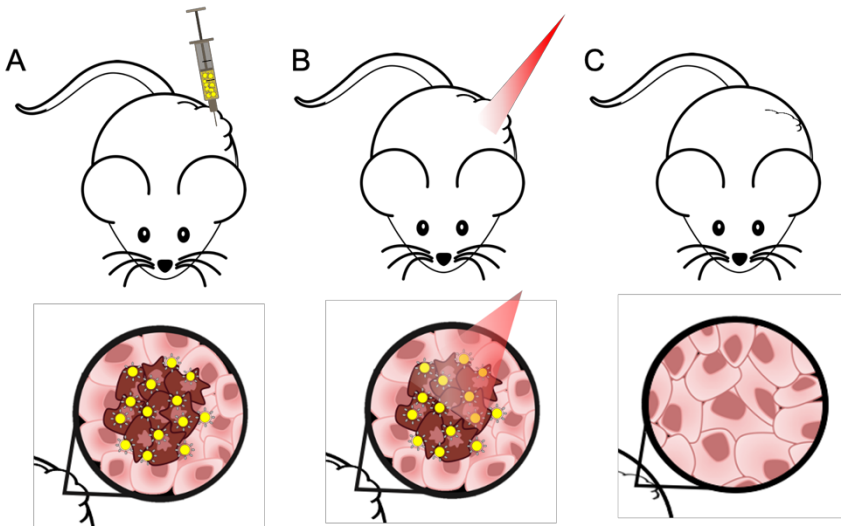

Figure 2. Different steps of PTT using a targeted hybrid gold-based nanosystem developed and a near-infrared (NIR) laser, in a xenograft mice model. **(A)** *In situ* administration of hybrid nanosystem at the tumor site, specific for tumor cells (represented in a darker color); **(B)** Irradiation of the injected site with a NIR laser to activate the formulation; **(C)** Reduction of tumor mass through thermal ablation.

Some of these therapeutic results displayed much higher response rates in comparison to the current therapies used, being 10 months the longest overall survival rate reported. The 2-3-fold increase in overall survival corresponds to less than a year.

Table 3 resents ongoing clinical trials (Phase I and II) registered on the ClinicalTrials.gov database, and its respective database ID, being conducted worldwide, using different treatment approaches and protocols (*i.e.,* radiotherapy, chemotherapy, immunotherapy, small-molecule tyrosine kinase inhibitors, and a combination of these therapies) for the treatment of anaplastic thyroid carcinoma.

Table 2. Results of completed clinical trials using targeted or multi-target therapies for the treatment of anaplastic thyroid carcinoma.

Drug	Target	Main Outcomes	Reference
Everolimus	mTOR	PFS of 47 weeks; 63% of patients reported tumor shrinkage.	[166]
Vemurafenib	BRAF	Complete clearance of metastasis 38 days after treatment	[164]

Sunitinib	Multi-targeted (*i.e.,* RET, VEGFR)	Significant decrease of neck mass, alleviating symptoms	[167]
Dabrafenib + Trametinib	BRAF and MEK, respectively	69% response rate	[165]
Imatinib	Multi-targeted (*i.e.,* Bcr-Abl, c-kit)	45% of patients had 6-months OS	[168]
Lenvatinib	Multi-targeted (*i.e.,* VEGFR, FGFR, PDGFRα, RET, KIT)	PFS of 7.4 months OS of 10.6 months	[107]
Sorafenib	Multi-targeted (*i.e.,* VEGFR, RET, Raf, PDGFR)	PFS of 77 weeks	NCT00654238 (clinicaltrials.gov)

PFS – Progression-Free Survival and OS – Overall Survival

Table 3. Ongoing clinical trials using targeted or multi-targeted therapies, radiotherapy, immunotherapy and chemotherapy for the treatment of anaplastic thyroid carcinoma.

Drug	Target	ClinicalTrials.gov ID	Phase
Lenvatinib	Multi-Targeted (*i.e.,* VEGFR, FGFR, PDGFRα, RET, KIT)	NCT02726503	II
Trametinib + Paclitaxel	MEK, BRAF	NCT03085056	Early I
Durvalumab + Tremelimumab + Stereotactic Body Radiotherapy	PD-1 and CTL-4, respectively	NCT03122496	I
MLN0128	mTOR	NCT02244463	II
Pembrolizumab	PD-1	NCT02688608	II
Nexavar	Multi-Targeted (*i.e.,* RAF, MEK, ERK, VEGFR, PDGFR)	NCT03565536	II
Efatutazone + Paclitaxel	PPAR γ	NCT02152137	II
Intensity-Modulated Radiation Therapy + Paclitaxel + Pazopanib Hydrochloride	Multi-Targeted (*i.e.,* VEGFR, PDGFR, c-kit)	NCT01236547	II

Atezolizumab + Bevacizumab + Cobimetinib + Paclitaxel + Vemurafenib	PD-1, VEGFR, MEK and BRAF, respectively	NCT03181100	II

Although some advances have been done regarding the treatment of anaplastic thyroid carcinoma, it still presents low survival rates. There is an urgent need to improve the treatment of this rare malignancy, in order to significantly increase patients' survival and their life quality improvement. Altogether, the best approach seems to be a more personalized multimodal course of treatment, since there is considerable variability of response to treatments using targeted/multi-targeted therapies between individuals with tumor molecular profile.

2. Objectives of this project

This project aims to develop, characterize and assess the efficacy of a novel formulation of targeted and biocompatible AuNPs, for PTT of anaplastic thyroid carcinoma, a superficial, and very lethal, tumour.

The group has previously developed a novel formulation of functionalized AuNPs, with a polymeric coating composed of Hyaluronic Acid and Oleic Acid (HAOA), to specifically treat melanoma with AuNP-mediated NIR-PTT [58,161]. The specificity is a consequence of the functionalization with EGF, the ligand of EGFR, generally overexpressed in human melanoma cells [169]. This functionalization is also efficient due to the coatings' (HAOA) strong adsorbing capacity, as already described by the same research group. This formulation had very promising preliminary results [58,161]. To treat anaplastic thyroid carcinoma, the previously formulated coated-AuNPs formulation was modified and, by changing its' ligands, a novel formulation specific for anaplastic thyroid carcinoma can be developed.

Like stated in section 1.3.2, as both EGFR and TfR1/CD71 membrane receptors are overexpressed in anaplastic thyroid carcinoma, it is possible to target these cancer cells by functionalizing the novel coated-AuNPs formulation with ligands for these receptors. Thus, different ligands will be studied to try and maximize the formulations' efficacy, including EGF and lapatinib, both targeting EGFR, and holo-transferrin (HTf), targeting TfR1/CD71, overexpressed in anaplastic thyroid carcinoma.

Firstly, a novel formulation of AuNPs must be designed and characterized regarding its physicochemical properties (*i.e.,* mean size and size distribution, conjugation efficiency, absorbance spectra and morphology). Furthermore, the AuNPs will be coated and functionalized with each of the selected ligands, and the most appropriate ligand will be then chosen regarding the results of different studies, such as the overall physicochemical properties and *in vitro* assessments. Using non-cancerous and anaplastic thyroid carcinoma commercialized cell lines, safety, selectivity and efficacy of the different coated and functionalized formulations will be assessed, when activated and not-activated, using cell viability studies. After optimization, the most adequate ligand will be selected, and the safety and biodistribution of the coated and functionalized AuNPs will be assessed *in vivo*, using CD-1 mice. For this, the final formulation will be administered to mice, and biochemical and histologic assessments will be conducted, as well as the gold content in the different tissues, and tissue indexes, will be determined.

3. Materials and Methods

3.1 Materials

3.1.1 Reagents

Gold (III) chloride trihydrate, Silver Nitrate, L-ascorbic Acid, Hyaluronic Acid (HA), Rosmarinic Acid (RA), Oleic Acid (OA), holo-Transferrin human (powder, grade 97%) and Lapatinib (98%) were acquired from Sigma-Aldrich (St. Louis, MO, USA). EGF Recombinant Human Protein was supplied from Gibco (ThermoFisher Scientific, Waltham, MA, USA). Bradford Dye Reagent was purchased from Alfa Aesar (ThermoFisher Scientific, Waltham, MA, USA). Water MilliQ by Merck Millipore (Burlington, MA, USA). All chemical products and solvents used were of analytical purity grade.

3.1.2 Cell lines and cell culture

Cell growth was done according to supplier's instructions (ATCC). The human keratinocyte cell line HaCat was maintained in Dulbeco's modified Eagle's medium (DMEM), with high-glucose (4500 mg/mL), complemented with 100 µg/mL penicillin/streptomycin and 10% foetal bovine serum (FBS). Human anaplastic thyroid carcinoma cell line 8505C was maintained in RPMI 1640, and supplemented as previously mentioned for DMEM. All cell lines were stored in a humidified chamber at 37ºC, in a 5% CO_2 atmosphere. The cell cultures were maintained every 2 to 3 days, at which the medium was changed, until a confluence of 80% was achieved.

3.1.3 Animals

Male CD1 mice were purchased from IHMT (Lisboa, Portugal). The animal housing was kept at the controlled temperature of 22.0 ± 1.0ºC, humidity at 50.0 ± 15.0% and a cycle of light of 12h in Faculty of Pharmacy facilities. Animals were kept under standard hygiene conditions, fed commercial chow and given acidified drinking water *ad libitum*.

All experiments regarding the usage of animals were conducted in accordance with the EU Directives (2010/63/UE), the Portuguese Law (DL 113/2013, 2880/2015 and 260/2016), and were approved both by the Animal Welfare Body (ORBEA) of the Faculty of Pharmacy, University of Lisbon, and of the Ethics Committee of the NOVA Medical School, Faculdade de Ciências Médicas, NOVA University Lisbon .

3.2 Methods

3.2.1 Preparation of HAOA-coated AuNPs

The HAOA-coated AuNPs were prepared using a modified approach previously published by our group [161]. The full process is still under patent protection (WO 2017/095251). Briefly, an aqueous solution of gold (III) chloride trihydride was mixed with an aqueous solution containing L-ascorbic acid, silver nitrate and RA. The mixture was continuously stirred for 15 min (800 rpm, Heidolph MR3001, Heidolph Instruments, Schwabach, Germany), at room temperature. Two different ratios of gold:RA (m/m) were tested, 5:3 and 5:10, originating two different AuNPs' cores.

The HAOA coating was prepared by adding, while stirred at 400 rpm, at 60ºC, the following to milli-Q water: hyaluronic acid (HA), oleic acid (OA) and sodium hydroxide. This aqueous mixture is stirred overnight at the mentioned conditions. In order to coat the AuNPs' core, the HAOA prepared overnight is cooled to room temperature, and is mixed with the AuNPs' core solution, 1:1 (v/v). The method of functionalization of the HAOA-coated AuNPs is the same regardless of the ligand (*i.e.,* EGF, HTf, lapatinib), by mixing the HAOA-coated AuNPs with the phosphate buffered saline pH 7.4 (PBS, according USP32) solution containing the intended ligand under magnetic continuous stirring, for 30 min at room temperature, at a ratio of 1:1 (v/v).

In order to recover AuNPs, suspension was centrifuged at 7200 x g, for 15 min (Beckman Instruments centrifuge, Inc., Brea, CA, USA). The supernatant was stored in order to determine the efficiency of ligand conjugation to the NPs, and the pellet, correspondent to the functionalized HAOA-coated AuNPs, was resuspended in PBS and stored at -4ºC.

3.2.2 HAOA-coated AuNPs characterization

a) Mean Size and Polydispersivity Index (PdI)

The different formulations, AuNPs core and HAOA-coated AuNPs, functionalized with the different ligands and non-functionalized, were characterized regarding its mean size and polydispersivity index (PdI). The formulations were diluted in PBS pH 7.4 (1:10, v/v). Zetasizer Nano ZS (Malvern Instruments, Malvern, UK) was used to measure mean size and PdI, using Dynamic Light Scattering. All measurements were performed in triplicate.

b) Determination of Conjugation Efficiency

To determine the conjugation efficiency (%) of the different HAOA-coated AuNPs functionalized formulations (*i.e.,* EGF-functionalized, HTf-functionalized and lapatinib-functionalized HAOA-coated AuNPs) the different formulations were centrifuged, at 7200 x g for 15 min, as mentioned, and the supernatant was stored. Different methods were used to determine the concentration of ligand present in the formulations' supernatant, and after this concentration was determined, the conjugation efficiency was calculated using the following equation 1:

$$\text{Conjugation Efficiency (\%)} = \frac{Ligand\ Concentration\ \text{in}\ the\ Supernatant}{Concentration\ of\ ligand\ solution\ used\ to\ initially\ prepare\ NPs} \times 100 \quad \text{(Eq. 1)}$$

i. Determination of EGF's concentration in the supernatant

To determine the concentration of EGF present in the supernatant of EGF-functionalized HAOA-coated AuNPs, after centrifugation, the following Bradford protocol was employed. Firstly, BSA solutions, with concentrations ranging from 0 to 25 µg/mL, were prepared in order to plot the calibration curve. Then, the sample/calibration curve solution were mixed with ThermoFisher Bradford Solution (ThermoFisher Scientific, Waltham, MA, USA) in a 96-well microplate, at a ratio of 1:1 (v/v), and left to incubate for 5 min. After this time period, the absorbance of the 96-well microplate was measured using a BioTekTM ELx800™ Absorbance Microplate Reader (Winooski, VT, USA), at 570 nm. The absorbance was then converted into concentration using the equation 2 plotted with the calibration curve solutions (R^2 = 0.9801). This was then applied to equation 1, allowing the determination of the conjugation efficiency. All measurements were performed in triplicate.

$$Abs = 0.0022 \times EGF_{Concentration} + 0.0331 \quad \text{(Eq. 2)}$$

ii. Determination of HTf concentration in the supernatant

The concentration of HTf present in the supernatant obtained from the centrifugation of HTf-functionalized HAOA-coated AuNPs was determined by using the A280 function in ThermoFisher NanoDrop™ ND-1000 UV-Vis Spectrophotometer (ThermoFisher Scientific, Waltham, MA, USA). For this, a droplet (2µL) of the supernatant was placed in the equipment pedestal and the measurement was carried out. The obtained concentration was then applied to equation 1, to determine the percentage of HTf that conjugated to the HAOA-coated AuNPs. All measurements were performed in triplicates.

iii. Determination of Lapatinib concentration in the supernatant

In order to determine the conjugation efficiency of lapatinib, the concentration of this drug present in the supernatant was determined by HPLC (Hitachi System LaCrom Elite, Column oven, Diode Array Detector UV-vis and Pump, Tokyo, Japan), following a protocol described elsewhere [170]. The supernatants were analyzed using a Columns Water Symmetry C18 (5 µm, 4.6 x 150 mm), with isocratic flow of 0.5 mL/min, and a mobile phase composed of acetonitrile/ water (70:30; v/v). Measurements were performed in triplicates at 227 nm, and a calibration curve was stablished using standardized solutions of lapatinib. The determined concentration was applied to equation 1, in order to determine the conjugation efficiency of lapatinib to the surface of the HAOA-coated AuNPs.

c) Surface and Morphology Analysis

The surface morphology of the different formulations, AuNPs' core and HAOA-coated AuNPs, functionalized with different ligands, and non-functionalized, was analyzed using Transmission Electron Microscopy (TEM). For TEM observations, aliquots (10 µL) of the aqueous suspensions of the different AuNPs formulations were carefully placed on 200-mesh copper grids previously coated with Formvar and carbon and left to adsorb for 1-3 min. After removing the excess of the samples with filter paper, the material was negative staining with 1.0% uranyl acetate for some minutes at room temperature, and further allowed to air-dry. Observations were made on a JEOL 1200EX transmission electron microscope (JEOL Ltd., Tokyo, Japan) operating at 80 kV. Images were recorded digitally

3.2.3 Determination of Absorbance Spectra of the HAOA-coated AuNPs

The maximum absorbance wavelength for the AuNPs' core, HAOA-coated AuNPs and functionalized HAOA-coated AuNPs were determined by scanning the formulations' absorbance at wavelengths raging from 400 to 1000 nm, using a UV-Vis Spectrophotometer (Hitachi, Tokyo, Japan), against a blank. Formulations were diluted in PBS at pH 7.4 (1:4; v/v). The measurements were performed in triplicate.

3.2.4 Determination of Recovery Yield

Prior to being recovered, all formulations (core, coated and functionalized) were centrifuged (7200 x g, 15 min) and freeze-dried using a FreeZone 2.5 Liter Benchtop Freeze Dry System (Labconco, Kansas City, MO, USA), at -49ºC for 48h. After lyophilization, the

powder was weighted and the recovery yield (RY, %) was calculated by using the following equation 3:

$$\text{Recovery Yield (\%)} = \frac{Final\ mass\ of\ AuNPs}{Initial\ mass\ of\ all\ components\ used\ in\ formulation} \times 100 \qquad \text{(Eq. 3)}$$

3.2.5 In vitro Safety Assessment

Safety was *in vitro* assessed by evaluating cell viability (methylthiazolyldiphenyl-tetrazolium bromide, MTT, assay) of the healthy cell line HaCat, after incubation with the different formulations, when not activated by laser. For this, HaCat cells were seeded in a 96-well plate at a concentration of 7.5 x 10^4 cells/well, and left to incubate with the formulations, for 24 h, at 20 µM and 80 µM: core AuNPs, HAOA-coated AuNPs, EGF-functionalized HAOA-coated AuNPs, HTf-functionalized HAOA-coated AuNPs, lapatinib-functionalized HAOA-coated AuNPs, and the free ligands (EGF, HTf and lapatinib). After 24 h, the formulations-containing medium was removed, the cells were washed twice with PBS pH 7.4, and 200 µL MTT reagent (Sigma-Aldrich, St. Louis, MO, USA) was added, at a concentration of 0.5 mg/mL (in complete DMEM). The cells were then left to incubate with the MTT reagent for 4h, in order to allow the crystals to form and, after the time period passed, the crystals were solubilized using dimethyl sulfoxide (DMSO). Absorbance was measured using a BioTekTM ELx800TM Absorbance Microplate Reader (Fisher Scientific, NH, USA), at 570 nm. The control wells (no treatment) were considered as 100% viable. The results are presented as percentage of the control wells and calculated according with equation 4:

$$Cell\ Viability\ (\%) = \frac{Abs_{test\ group}}{Abs_{control}} \times 100 \qquad \text{(Eq. 4)}$$

3.2.6 In vitro Efficacy Assessment

Efficacy was assessed *in vitro* by MTT assay. Human anaplastic thyroid carcinoma cell line 8505C were seeded in two mirroring 96-well plate at a concentration of 7.5 x 10^4 cells/well, and left to incubate with the formulations (AuNPs, HAOA-coated AuNPs, EGF-functionalized HAOA-coated AuNPs, HTf-functionalized HAOA-coated AuNPs and lapatinib-functionalized HAOA-coated AuNPs), for 4 h, at 80 µM. After 4 h, the formulation-containing media was removed and substituted with fresh medium, and one of the plates containing the cells were irradiated with a laser emitting at 808 nm, 3A, for 3 min, as shown in Figure 3, and the other plate was left without being irradiated. To control the possible cytotoxicity of the laser, cells that were not incubated with formulations were also irradiated. The cells were washed twice with PBS at pH 7.4, and 200 µL MTT reagent (Sigma-Aldrich, St. Louis, MO, USA) was

added, at a concentration of 0.5 mg/mL (in complete RPMI). The cells were then left to incubate with the MTT reagent for 4h, in order to allow the crystals to form, posteriorly solubilized using DMSO. Absorbance was measured using a BioTekTM ELx800TM Absorbance Microplate Reader (Fisher Scientific, NH, USA), at 570 nm. In similarity to the previous MTT assay, the control wells (no treatment) were considered as 100% viable. The results were also calculated using equation 4 and presented as percentage of controls.

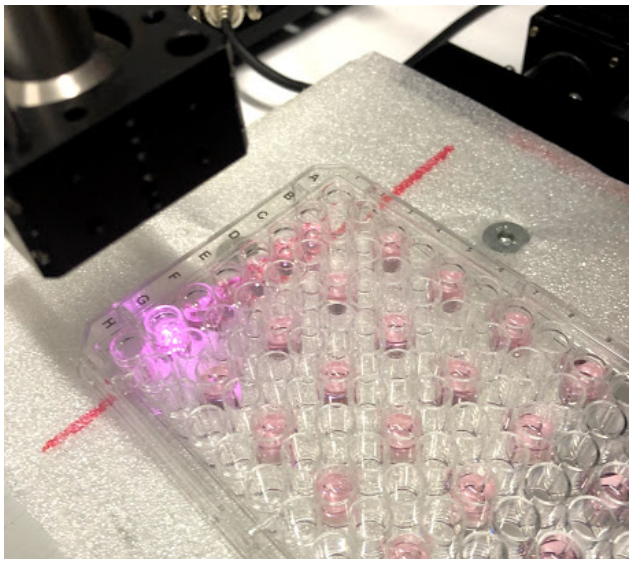

Figure 3. Laser setup for *in vitro* activation of gold nanoparticles (AuNPs).

3.2.7 In vitro Selectivity Assessment

Selectivity of the formulations was tested *in vitro* by determining the viability of 8505C cells after incubation with the different formulations for 24 h and comparing to the results of the *in vitro* safety assessment using HaCat cells. For this, the cells were seeded in a 96-well plate at a concentration of 7.5 x 10^4 cells/well, and left to incubate with the formulations (AuNPs, HAOA-coated AuNPs, EGF-functionalized HAOA-coated AuNPs, HTf-functionalized HAOA-coated AuNPs and lapatinib-functionalized HAOA-coated AuNPs), for 24 h, at 20 µM and 80 µM. After this time period, the cells were washed twice with PBS pH 7.4, and 200 µL MTT reagent (Sigma-Aldrich, St. Louis, MO, USA) was added, at a concentration of 0.5 mg/mL (in complete RPMI). The cells were then left to incubate with the MTT reagent for 4 h and the crystals were solubilized using DMSO. Absorbance was measured using a BioTekTM ELx800TM Absorbance Microplate Reader (Fisher Scientific, NH, USA), at 570 nm. In similarity to the previous MTT assays, the control wells (no treatment) were considered as 100% viable, and the results, in percentages, were calculated using equation 4.

3.2.8 In vitro haemolytic activity

The used protocol was based on a previously published one [171]. Briefly, ethylenediamine tetraacetic acid (EDTA)-preserved peripheral human blood was collected from voluntary donors at the day of the determination of the haemolytic activity of AuNPs core, HAOA-coated AuNPs and HTf-functionalized HAOA-coated AuNPs. The peripheral blood was centrifuged at 1000 x g, for 10 min, in order to separate and remove the plasma from the erythrocytes. After this, the erythrocyte pellet was suspended in PBS and centrifuged at 1000 x g, for 10 min, allowing the pellet to be washed three times. The formulations were diluted in PBS to concentrations ranging from 0.04 to 80 μM (2-fold dilution). One hundred μL of the diluted formulations were added to wells of 96-well plates, adding 100 μL of the erythrocyte suspension to the formulation-containing wells. Erythrocytes and distilled water were added to wells, correspondent to total haemolysis (positive control), and erythrocytes and PBS were added to other wells (negative control). The plate was left to incubate for 1 h and was then centrifuged at 800 x g, for 10 min. The supernatants were collected and the absorbance (Abs) was measured using a BioTekTM ELx800^{TM} Absorbance Microplate Reader (Winooski, VT, USA), at 570 nm, with a reference filter of 620 nm. The haemolytic activity (%) was determined according to the following equation 5:

$$\text{Haemolytic Activity (\%)} = \frac{Sample\ Abs - Negative\ Control\ Abs}{Negative\ Control\ Abs - Positive\ Control\ Abs} \times 100 \qquad \text{(Eq. 5)}$$

3.2.9 Preliminary in vivo Assessment of HTf-functionalized and non-functionalized HAOA-coated AuNPs

a) In vivo preliminary safety assessment

An *in vivo* preliminary safety assessment of the HAOA-coated AuNPs was performed using CD1 mice, with a mean weight of 23 g (n=18). The formulation was subcutaneously (s.c.) administered in the thyroid neck region, at a dosage of 23 mg/kg of body weight. Although the dosage administered was based on previous works by other groups [172], the dose to be administered, although intravenous, is not consensual, with groups reporting 1 mg/kg of body weight, while others suggest 20 mg/kg of body weight [172–174]. Then, the animals were randomly separated into six groups, each with 3 specimens, being sacrificed at different time points: 30 min (group 1), 1 h (group 2), 2 h (group 3), 4 h (group 4), 6 h (group 5) and 24 h (group 6). At each time point, the animals of each group were anesthetized and sacrificed, according to animal welfare principles. Afterwards, peripheral blood samples were collected for biochemical analysis, pictures of the neck region were taken, and organs and

tissues (*i.e.,* neck region including thyroid, spleen, right lobe of the liver, right kidney, skin from administration site) were harvested for histological analysis. For biochemical analysis, plasma has to be separated from whole blood. In order to do this, the collected blood was centrifuged at 1000 x g, for 10 min, and the supernatant, corresponding to plasma, was collected for quantification of IL-6, ALT (to determine liver toxicity), creatinine and urea (to determine kidney toxicity).

The organs and tissues harvested were prepared for histological analysis by being fixed in 10% formalin and embedded in paraffin. Then, the specimens were sectioned (5 μm sections) and stained with hematoxylin-eosin. The histologic preparations were observed in an Olympus BX51 microscope (Olympus Corporation, Tokyo, Japan). An Olympus U-TV1X-2 colour camera was used to capture representative images of the preparations.

b) In vivo biodistribution assessment of HTf-functionalized HAOA-coated AuNPs

The biodistribution of HTf-functionalized HAOA-coated AuNPs and HAOA-coated AuNPs was *in vivo* assessed using CD-1 mice (n=12). The animals were randomly distributed for different groups and administered either HTf-functionalized HAOA-coated AuNPs or HAOA-coated AuNPs. In similarity to the previous assay, the respective formulation was administered s.c. in the thyroid region at a dose of 23 mg/kg of body weight. The animals of each group were then re-divided into two subgroups, according to the time point at which they would be scarified: 4 h post-administration; and 24 h post-administration. Respecting the animal welfare principles, the animals were sacrificed and the main organs involved in clearance and excretion (*i.e.,* liver, spleen, kidneys and lungs) were harvested and weighed, in order to determine its' tissue indexes, at 4 h and 24 h post-administration of HAOA-coated AuNPs or HTf-functionalized HAOA-coated AuNPs, according to the following equation 6 [175]:

$$Tissue\ Index = \sqrt{\frac{organ\ weight}{animal\ weight}} \times 100 \qquad \text{(Eq. 6)}$$

After weighting the organs, Inductively Coupled Plasma-Mass Spectrometry (ICP-MS) was conducted in order to determine the amount of Hf-functionalized HAOA-coated AuNPs and HAOA-coated AuNPs present in each of these organs (*i.e.,* liver, spleen, kidneys and lungs) as well as in the blood. For this analysis, the organs and blood were freeze dried and stored at -80ºC and further digested using a microwave digestive system and a mixture of nitric acid and hydrochloric acid (5% of each).

3.2.10 Statistical Analysis

Data is presented as mean ± SD, with a $n \geq 3$. GraphPad Prism Version 5.03 (GraphPad Software, San Diego, CA, USA) was used to perform all the statistical analysis. Statistical differences were evaluated with ANOVA, and the differences were considered as significant for $p < 0.05$.

4. Results

4.1 Optimization and characterization of the functionalized HAOA-AuNPs

4.1.1 Mean size and Polydispersivity index (PdI)

AuNPs were prepared using two different ratios of gold:RA, 5:3 and 5:10 (m/m). The AuNP core (Figure 4A) was formulated following the presented ratios, and the NPs were coated with the novel HAOA coating (Figure 4B). Mean size and PdI were determined throughout the different steps of assembling the final formulation (*i.e.,* core synthesis, coating of the NPs and functionalization of the AuNPs surface), and the results are presented in Table 4. Looking at the results regarding the size of the uncoated AuNPs, AuNPs' size varied significantly when different gold:RA ratios (m/m) were used, and tended to increase when the HAOA coating was added, for both AuNPs formulated using 5:3 (increase of ~40%) and 5:10 (increase of ~12%) (m/m) gold:RA ratios, suggesting that the AuNP's core was successfully coated. Concerning all results, the 5:10 AuNPs core was then chosen for functionalization using three different ligands: EGF, HTf and Lapatinib (Figure 4C). After functionalization, mean size and PdI were determined once more, and it is to note that there was a tendency of increase in size, significant in the case of the EGF-functionalized HAOA-coated AuNP.

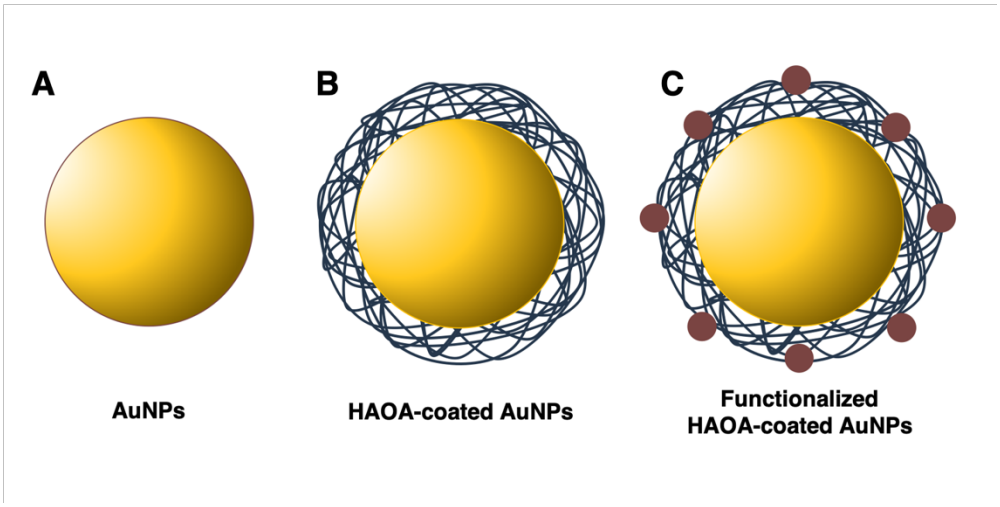

Figure 4. Gold nanoparticles (AuNPs) throughout the formulation processes: **(A)** AuNPs' core; **(B)** HAOA-coated AuNPs; and **(C)** functionalized (*i.e.,* EGF, HTf or lapatinib) HAOA-coated AuNPs.

Table 4. Mean size and polydispersivity index (PdI) of both 5:3 and 5:10 gold nanoparticles (AuNPs), throughout the different steps of the formulation. Data is presented as mean ± SD, n > 3 (** p<0.01, *** p<0.001).

	Sample	Mean Size (nm)	PdI
5:3 AuNPs	Uncoated	88.0 ± 11.6	0.319 ± 0.061
	HAOA-coated	125.3 ± 25.7	0.312 ± 0.072
5:10 AuNPs	Uncoated	314.7 ± 42.9 ***	0.475 ± 0.029
	HAOA-coated	354.0 ± 29.3	0.394 ± 0.176
	EGF-HAOA-coated	671.5 ± 65.8 **	0.579 ± 0.058
	HTf-HAOA-coated	415.3 ± 47.4	0.375 ± 0.078
	Lap-HAOA-coated	483.4 ± 179.7	0.494 ± 0.072

4.1.2 Morphologic analysis

Morphology was assessed by Transmission Electron Microscopy (TEM). Results are shown in Figure 5 and include ratio 5:3 gold:RA (m/m), uncoated and HAOA-coated, while Figure 6 showcases the morphology analysis results of 5:10 gold:RA (m/m) ratio AuNPs, uncoated, HAOA-coated and functionalized using the three ligands (EGF, HTf and lapatinib).

In Figure 5A, it is to note the presence of NPs with different shapes (*i.e.,* spherical, triangular, truncated triangular and hexagonal-shaped AuNPs) and sizes. In Figure 5B, the 5:3 AuNPs were coated with HAOA, where we can see the black AuNP core surrounded by a white cloudy coating, probably related to the HAOA mixture.

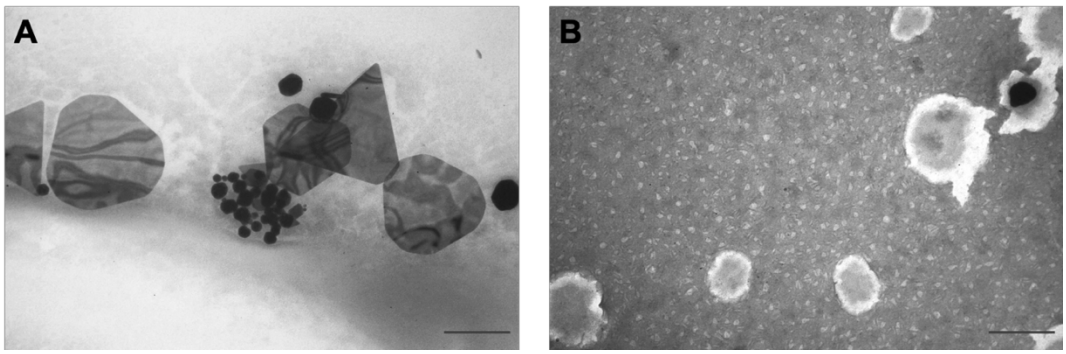

Figure 5. TEM micrographs of 5:3 gold:RA (m/m) gold nanoparticles (AuNPs): **(A)** uncoated and **(B)** HAOA-coated AuNPs. Scale bars = 200 nm.

Figure 6A shows the isolated uncoated core of 5:10 AuNP, with a very defined icosahedron-shaped AuNP. But, as previously seen for the 5:3 AuNPs, the shape of the 5:10 AuNPs changed after HAOA coating addition, seen in Figure 6B as spherical NPs. Figure 6C-E shows the spherical-shaped functionalized HAOA-coated AuNPs with: EGF, Figure 6C; HTf, Figure 6D; and lapatinib, Figure 6E. By observing Figure 6C, D and E, it is evident the increased size of the EGF-functionalized HAOA-coated AuNPs in comparison to the other AuNPs, as was confirmed by the size analysis.

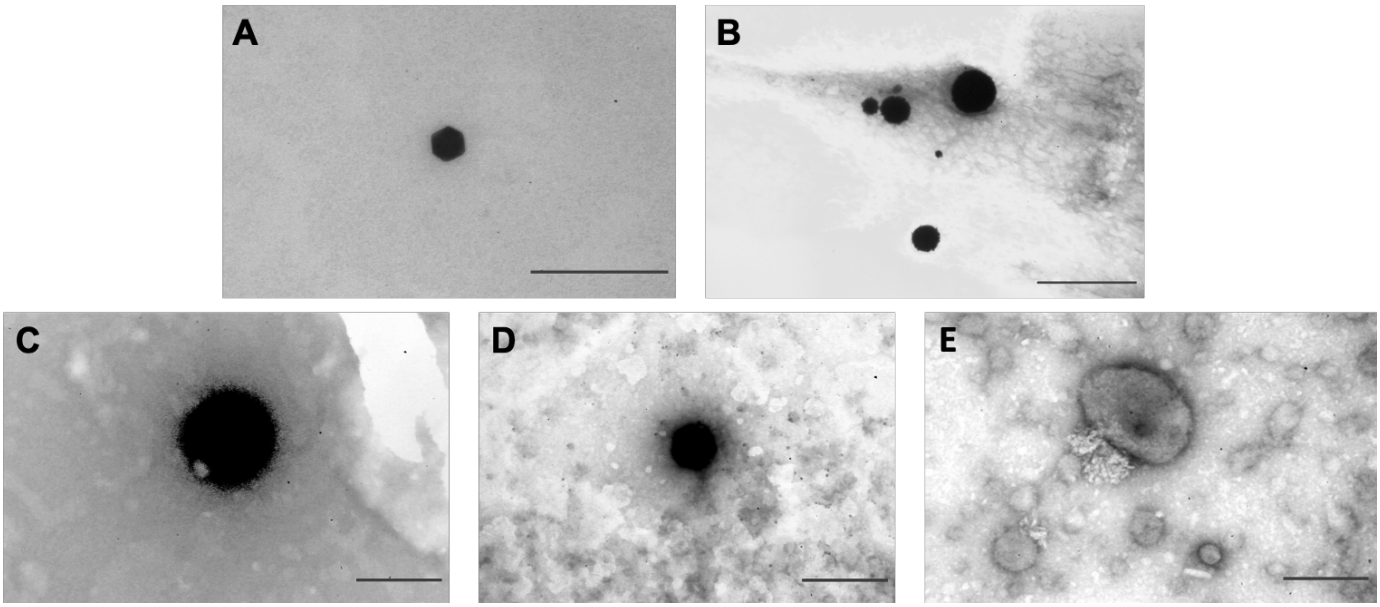

Figure 6. TEM micrographs of ratio 5:10 gold:RA (m/m) gold nanoparticles (AuNPs): **(A)** uncoated, **(B)** HAOA-coated, **(C)** EGF-functionalized HAOA-coated, **(D)** HTf-functionalized HAOA-coated and **(E)** Lap-functionalized HAOA-coated AuNPs. Scale bars = 200 nm.

4.1.3 SPR band

In order for the AuNP-mediated PTT to be more effective, the AuNPs must absorb at wavelengths in the biological windows (700-980 nm and 1000-1400 nm). Thus, the aim was to develop functionalized HAOA-coated AuNPs that absorbed in the NIR range (650-950 nm) of the light spectrum, as these wavelengths are described to safely penetrate healthy tissues and to allow the activation of AuNPs localized in less-superficial tumours [50], such as thyroid malignancies. To evaluate this, the SPR band, corresponding to the maximum absorbance peak (Abs_{max}) of the AuNPs was determined throughout the different steps of development, for both gold:RA ratios used (Table 5). It is worth notice that while 5:10 uncoated AuNPs present a SPR band in the NIR wavelengths, the 5:3 uncoated AuNPs did not, presenting a SPR band in the visible range of the light spectrum. It is to expect a shift to higher wavelengths when the

AuNPs were coated with HAOA. Although this was the case for the 5:10 HAOA-coated AuNPs, with a shift from 753 ± 54 to 840 ± 122 nm, it was not what was seen for the 5:3 AuNPs, which SPR band decreased from 551 ± 26 nm, when uncoated, to 536 ± 2 nm when coated with HAOA, remaining in the visible range. Due to this, the 5:10 AuNPs were chosen for the next stage of the formulation design: functionalization with the ligands. It is to note that after functionalization with the different ligands, the SPR band of the functionalized and coated 5:10 AuNPs shifts to lower wavelengths, with the Abs_{max} of the EGF- and HTf-functionalized HAOA-coated 5:10 AuNPs remaining in the NIR range (785 ± 127 and 710 ± 128 nm, respectively), but not the Abs_{max} lapatinib-functionalized HAOA-coated 5:10 AuNPs (481 ± 25 nm), which has shifted into the visible section of the light spectrum.

Table 5. SPR peak (Abs_{max}) of both 5:3 and 5:10 gold nanoparticles (AuNPs), throughout the different steps of the formulation. Data is presented as mean ± SD, n > 3.

	Sample	**SPR band (Abs_{max} nm)**
5:3 AuNPs	Uncoated	551 ± 26
	HAOA-coated	536 ± 2
5:10 AuNPs	Uncoated	753 ± 54
	HAOA-coated	840 ± 122
	EGF-HAOA-coated	785 ± 127
	HTf-HAOA-coated	710 ± 128
	Lap-HAOA-coated	481 ± 25

4.1.4 Recovery yield of the optimized ratio

In order to determine the industrial scalability of the optimized AuNPs core (5:10), the RYs of the formulations were determined, including the uncoated core, coating and functionalized formulation, and the results are shown in Table 6. HAOA-coated and EGF-functionalized HAOA-coated 5:10 AuNPs had the lowest RY while lapatinib-functionalized HAOA-coated 5:10 AuNPs had the highest RY, achieving a mean value of 86%.

Table 6. Recovery Yield (RY) of the optimized gold nanoparticles (AuNPs) core, throughout the different steps of formulation.

Sample		RY (%)
5:10 AuNPs	Uncoated	78.2 ± 9.6
	HAOA-coated	57.7 ± 5.9
	EGF-HAOA-coated	66.0 ± 0.9
	HTf-HAOA-coated	70.0 ± 3.4
	Lap-HAOA-coated	86.2 ± 36.5

4.1.5 Conjugation efficiency

Due to the favourable characteristics of the 5:10 AuNP core (*i.e.,* SPR band in the NIR range) when compared to the 5:3 AuNP, the 5:10 AuNP formulation was chosen for functionalization and further testing, and is from now on referred to as AuNPs in this section. Conjugation efficiency was determined indirectly by measuring the non-conjugated free protein present in the supernatant after centrifugation through colorimetric assays or spectrophotometry for protein quantification, regarding EGF and HTf, and the results are summarized in Table 7. HTf-functionalized HAOA-coated AuNPs had a higher conjugation efficiency than the EGF-functionalized HAOA-coated AuNPs. The quantification of the non-conjugated free lapatinib by HPLC is still ongoing and, consequently, the determination of conjugation efficiency for this ligand is pending.

Table 7. Conjugation efficiency (%) of functionalized HAOA-coated 5:10 gold:RA (m/m) ratio gold nanoparticles (AuNPs) (mean value ± SD, n = 3).

Sample		Conjugation Efficiency (%)
HAOA-coated AuNPs	EGF-functionalized	77.51 ± 9.43
	HTf-functionalized	80.84 ± 8.72
	Lap-functionalized	ND

ND – Not determined (ongoing)

4.2 Preliminary safety assessment

In order to evaluate the *in vitro* safety of the different formulations for healthy tissues, HaCat cells were incubated with the non-laser activated formulations at two different concentrations (20 and 80 μM) for 24 h. The results of this *in vitro* assay are presented in Figure 7. There was significant decrease in cell viability for some of the treatments when compared

to the non-treated control (100%, not shown). However, since cell viability was higher than 70% for all tested formulations and concentrations, no significant cell death was observed. Regardless, addition of the HAOA coating seems to have improved cell viability when compared to the uncoated-AuNPs, for both concentrations, increasing cell viability by ~9% and ~17%, at 20 and 80 μM, respectively. Moreover, all of the functionalized (EGF, HTf and lapatinib) HAOA-coated AuNPs did not decrease cell viability bellow 85%, and thus seem to be safe for healthy tissues, *in vitro*.

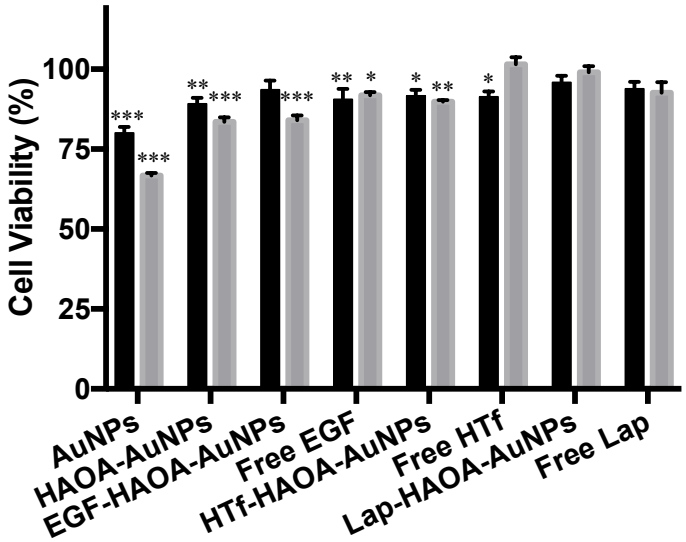

Figure 7. Cell viability (%) of HaCat cells after a 24 h incubation period with the different formulations of gold nanoparticles (AuNPs) (coated and uncoated, and functionalized with the different ligands and non-functionalized) at two different concentrations (20 μM, in black and 80 μM, in grey). Results are shown regarding mean ± SD, n = 5 (* $p < 0.05$, ** $p < 0.01$, *** $p < 0.001$ vs control).

4.3 <u>In vitro efficacy assessment</u>

Efficacy of the formulation against anaplastic thyroid carcinoma was assessed using 8505C cells, a human anaplastic thyroid carcinoma cell line. For this, cells were incubated with the different formulations at 80 μM for 4 h, in order to allow the formulation to target the cells, bind cellular receptors and to be internalized by them. Cells were then irradiated with a laser to activate the formulations, emitting at 808 nm, with 3A, for 3 min, and cell viability was determined. The 8505C cells were incubated with the same formulations, not-activated, to compare the activity of the formulations after activation. Moreover, to ensure that the difference in viability seen was not caused by the laser, cells were left untreated and were irradiated, enabling to evaluate the solo effect of the laser in cell viability. The cell viability

results regarding the formulation efficacy are shown in Figure 8. All laser-activated treatments caused a significant decrease in 8505C cell viability when compared to the respective non-activated formulations. Furthermore, it was clear that the HTf-functionalized HAOA-coated AuNPs were the most cytotoxic for the anaplastic thyroid carcinoma cell line, both when activate and not-activated. Moreover, the laser had no effect over cell viability.

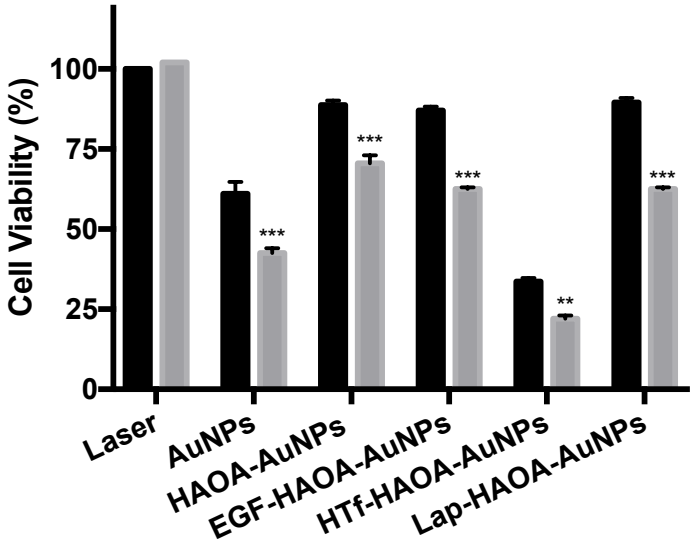

Figure 8. Cell viability (%) of 8505C cells, a human anaplastic thyroid carcinoma cell line, after a 4 h incubation period with the different formulations of gold nanoparticles (AuNPs) at 80 μM, activated with 3A (in grey) or not activated (in black) after this time period. Results are shown regarding mean ± SD, n = 3 (** $p < 0.01$, *** $p < 0.001$ vs control).

4.4 In vitro selectivity assessment

To complete the *in vitro* testing, the different AuNPs formulations' selectivity was assessed by incubating HaCat and 8505C cells with the different formulations at different concentrations (20 and 80 μM) for 24 h. Results are shown in Figure 9. By comparing the viability of both cell lines incubated with formulations at 20 μM (Figure 9A) for 24 h, it was observed that some formulations (*i.e.,* AuNPs, HAOA-coated AuNPs, EGF-functionalized HAOA-coated AuNPs and lapatinib-functionalized HAOA-coated AuNPs) were more cytotoxic for the HaCat cells than the cancerous 8505C cells, that seem to have shown some resistance to the formulations' action. In fact, the only formulation at 20 μM to which the 8505C were more susceptible was the HTf-functionalized HAOA-coated AuNPs, reducing 8505C cellular viability to 79.83 ± 3.36%, while HaCat cells' had a viability of 91.67 ± 1.87%. The results were slightly different when the formulations were more concentrated, at 80 μM (Figure 9B), as AuNPs and HTf-functionalized HAOA-coated AuNPs resulted in significantly different cell viability results

depending on the cell line, showing some selectivity for the anaplastic thyroid carcinoma cell line, inducing a more pronounced reduction in cell viability to the 8505C cells (34.83 ± 0.70% and 71.67 ± 2.06%, for each respective treatment) than to the HaCat cells (66.80 ± 0.80% and 89.83 ± 0.54%, for each respective treatment).

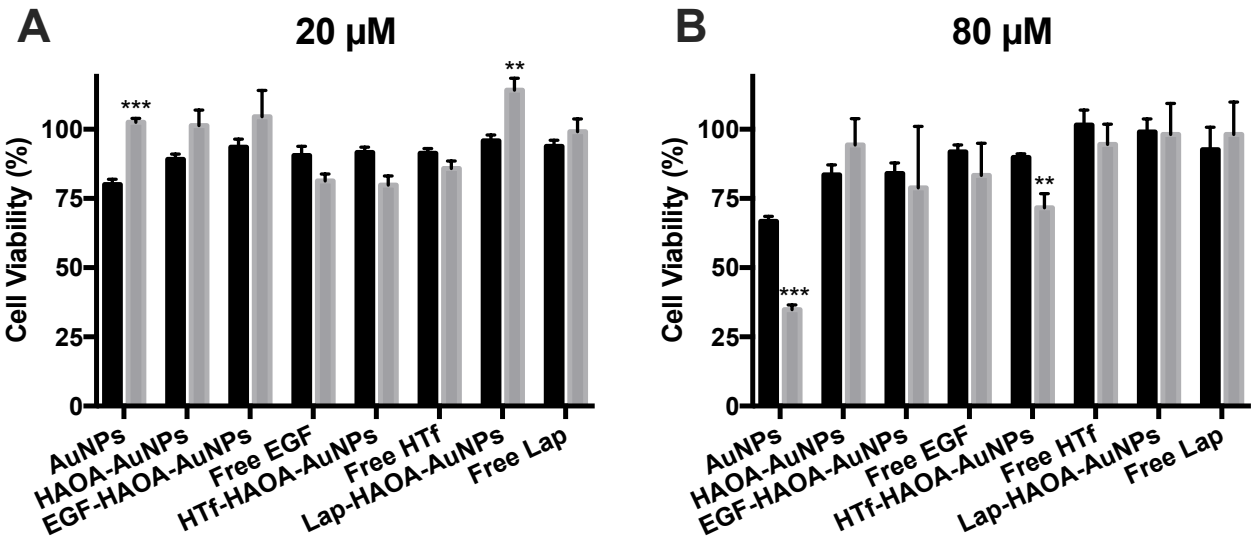

Figure 9. Cell viability (%) of healthy HaCat (black) and tumor cells 8505C (grey) cells after a 24 h incubation period with the different not-activated formulations of gold nanoparticles (AuNPs), at: **(A)** 20; and **(B)** 80 µM. Results are shown regarding mean ± SD, n = 5 (* $p < 0.05$, ** $p < 0.01$, *** $p < 0.001$ vs control).

Due to these and the previously presented *in vitro* results, HTf-functionalized HAOA-coated AuNPs was the formulation selected for the experiments moving forward.

4.5 In vitro haemolytic activity

The haemolytic activity of these formulations was determined at a range of different concentrations, using erythrocytes. Results are summarized in Figure 10. All concentrations resulted in a haemolytic activity lower than 2%, which is a good indicator for the safety and biocompatibility of all formulations, an important aspect to consider when using parenteral dosage formulations in future studies.

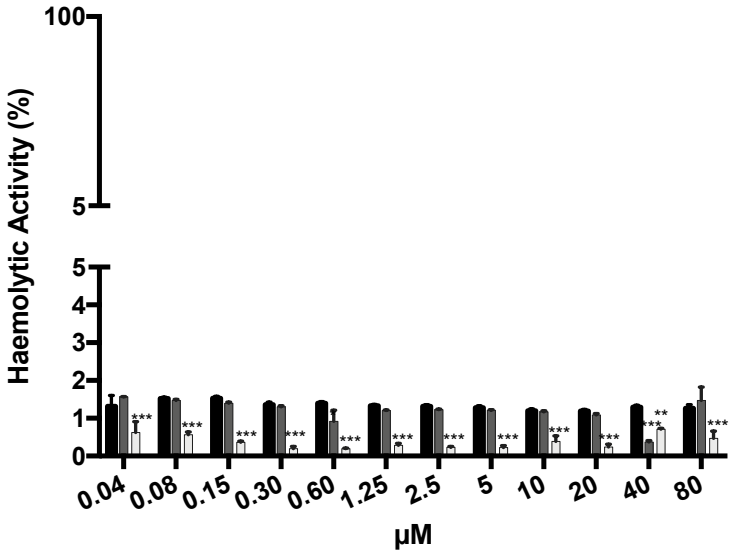

Figure 10. Haemolytic activity of gold nanoparticles (AuNPs) (black), HAOA-coated AuNPs (dark grey) and HTf-functionalized HAOA-coated AuNPs (light grey) at concentrations ranging from 0.04 to 80 μM. Results are shown regarding mean ± SD, n = 3 (* $p < 0.05$, ** $p < 0.01$, *** $p < 0.001$ vs control)

4.6 In vivo safety assessment

Figure 11 shows representative images of the different organs collected for *ex vivo* histological analysis from the different treatment groups. It was seen that the majority of the groups presented an accumulation of the HAOA-coated AuNPs (seen in a black-ish color) in the s.c. adipocyte tissue, adjacent to the administration site. Moreover, somehow the HAOA-coated AuNPs induced an inflammatory reaction with the presence of cellular infiltrates, more pronounced at 24h post-administration, mainly composed by macrophages and neutrophils, stained darker. These infiltrates suggest that macrophages might have phagocyted the HAOA-coated AuNPs. These observations were not done for group 2 and group 3, corresponding to 1 and 2 h, since no skin was present in the specimens, and thus, no subcutaneous fat. Regarding the other organs, no abnormalities were seen.

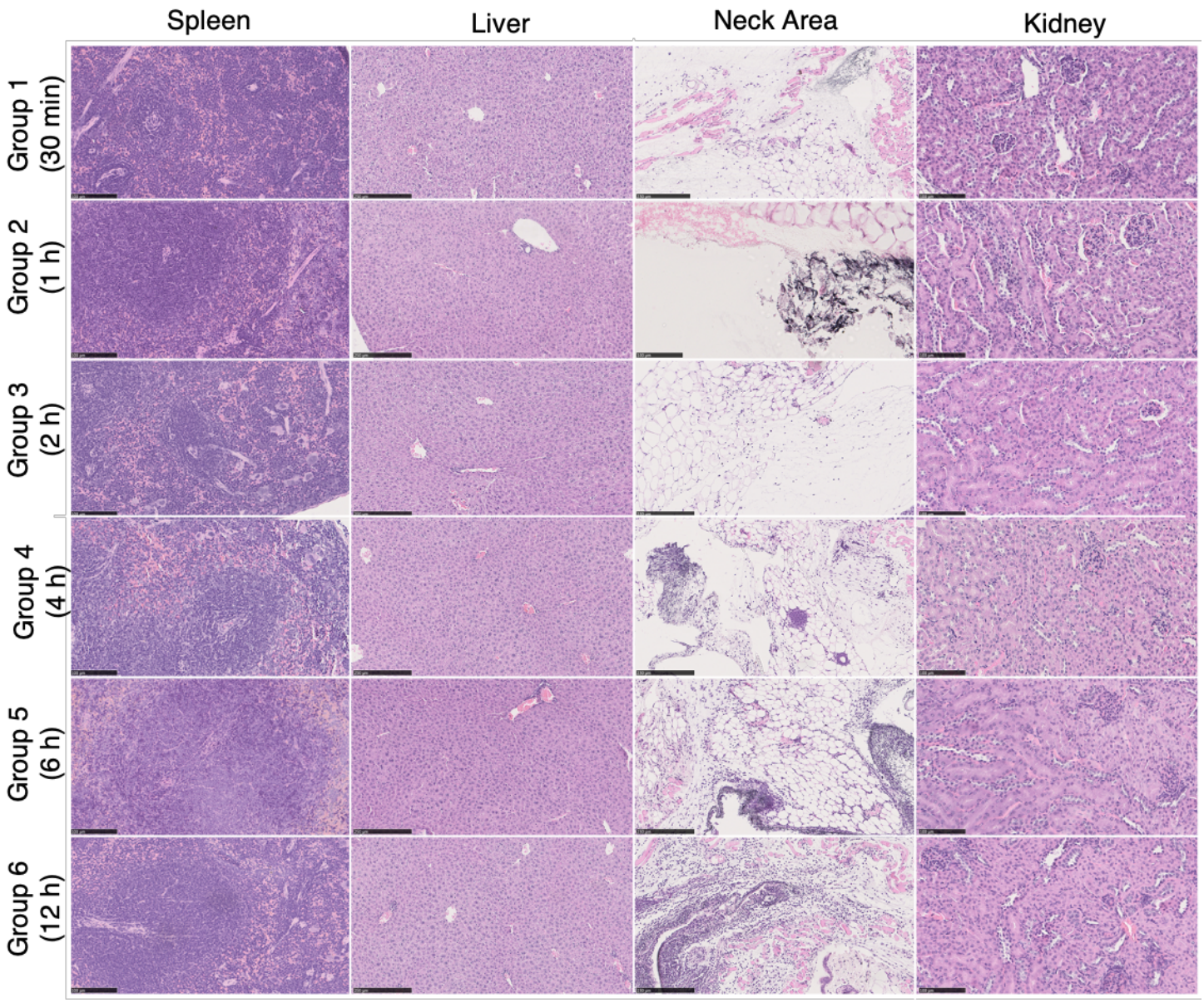

Figure 11. Histological images (spleen and kidney with 200× microscopic approach; liver and neck area with 100× microscopic approach) of the organs removed for analysis after necropsy (*i.e.,* spleen, liver, neck region, and kidney). For the neck region of 6 h and 12 h, it is possible to see cellular infiltrates of phagocytic cells, stained darker. All images are representative of the harvested organs, which showed no histologic alterations (H&E staining).

4.7 Preliminary in vivo biodistribution assessment

The tissue indexes of the main excretion organs (*i.e.,* liver, spleen, kidneys and lungs) were determined and the results are shown in Table 8. HAOA-coated AuNPs increased significantly the tissue index of the liver, at 24 h post-administration. However, the administration of HAOA-coated AuNPs did not result in other significant variations of tissue indexes. HTf-

functionalized HAOA-coated AuNPs led to an increase of the tissue index of the liver at both 4h and 24h post-administration, but this increase was more significant at 24 h. As for the non-functionalized formulation, HTf-functionalized HAOA-coated AuNPs did not trigger any other significant variations of the spleen, kidneys and lungs' tissue indexes.

Table 8. Tissue indexes (liver, spleen, kidneys and lungs) of mice at 4 h and 24 h post-s.c. administration of HAOA-coated and HTf-functionalized HAOA-coated gold nanoparticles (AuNPs). Control represents the tissue indexes of untreated animals. Results are presented as mean ± SD, n = 3 (* $p < 0.05$, ** $p < 0.01$).

Treatment		Tissue Index			
		Liver	Spleen	Kidneys	Lungs
Control		20.1 ± 0.1	6.0 ± 0.4	9.7 ± 0.1	7.2 ± 0.2
HAOA-coated AuNPs	4 h	20.4 ± 0.4	5.8 ± 0.5	10.1 ± 0.2	7.9 ± 0.2
	24 h	21.6 ± 0.6 *	6.3 ± 0.6	10.4 ± 0.1	7.7 ± 0.2
HTf-functionalized HAOA-coated AuNPs	4 h	21.4 ± 0.1 *	6.7 ± 0.2	10.5 ± 0.1	7.6 ± 0.3
	24 h	21.7 ± 1.0 **	6.7 ± 0.2	10.5 ± 0.2	8.0 ± 0.3

5. Discussion

Anaplastic thyroid carcinoma is one of the most lethal cancers known, presenting a mean survival of 3 to 5 months, with poor quality of life, currently without any efficient treatment option [176]. Moreover, the poor quality of life associated to cancer, in most patients, is not only due to the disease itself, but also caused by treatments' severe side effects, either associated to poor pharmacological properties or their invasiveness, *i.e.*, their effects in non-tumor cells.

Nanomedicine is an exponentially growing field and the application of nanoparticles, such as AuNPs, to the treatment of cancer has recently raised increasing interest. This is probably related to AuNPs attractive characteristics, such as their biocompatibility, stability, and low cytotoxicity, associated with the potential for high selectivity, which make them potentially suitable for treatment of cancer [22]. Additionally, several authors have reported that PTT-based approaches seem to be very promising for the treatment of superficial tumours [42,48]. Thus, non-pharmacological therapies mediated by NPs have been also explored, such as AuNPs-mediated NIR-PTT, with promising outcomes [60,61].

Since anaplastic thyroid carcinoma is a relatively superficial tumor, it is a more obvious candidate for AuNPs-mediated NIR-PTT. The formulation developed for AuNPs-mediated PTT of anaplastic thyroid carcinoma must be: small, monodisperse, highly selectivity, and thus be targeted for anaplastic thyroid carcinoma cells; biocompatible, to not harm healthy tissues; and effective, with high cytotoxicity, when activated by laser, for the anaplastic thyroid carcinoma cells to ensure tumour shrinkage.

5.1 Methodological considerations

In this project, the method used to produce AuNPs was adapted from the one previously developed by our group for the treatment of melanoma [58,161]. Furthermore, several formulations were assayed and parameters were tested: different cores of AuNPs were prepared using two ratios of gold:RA (m/m) (5:3 and 5:10), coated with HAOA and functionalized with three different ligands (EGF, HTf or lapatinib). In our preparation method, all the used compounds were generally regarded as safe for clinical application: gold (III) chloride trihydride and silver nitrate are not toxic and have been used for a long time for medical applications [177,178]; gold has the additional advantage of being an inert material [178]; L-ascorbic acid, also known as Vitamin C, is safe and metabolized by the human body, with growing interest due to its' potential intravenous administration for the treatment of cancer,

improving tumor response and survival [179]; and finally, the phytochemical RA, which has attracted more attention in the past few years due to some of its remarkable properties such as its antioxidant nature [180,181].

Several other methods for the preparation of AuNPs were described, such as the Turkevich method, seeding growth method, chemical method, the Brust-Schiffrin method, *e.g.* [182]. However, the majority of those methods synthetize AuNPs using cetyltrimethil ammonium bromide (CTAB), which is an inflammable and cytotoxic agent that raises important safety concerns [57,183]. Therefore, there was the need to develop CTAB-free AuNPs, either through using sophisticated removal methods to strip the CTAB from the AuNPs without disturbing the AuNPs' structure, or by using alternative agents for the AuNPs' synthesis. The method described in the present Dissertation was able to successfully overcome this challenge, as no CTAB was used.

Thus, by optimizing and adapting the previously described formulation [58,161], using nontoxic and safe compounds, we were able to develop safe and specific formulations for AuNPs-mediated NIR-PTT of anaplastic thyroid carcinoma.

5.2 Formulation characterization

The formulations were characterized in each step of production (*i.e.,* core synthesis, coating addition and functionalization of the AuNPs' surface) regarding its' size, PdI, SPR band correspondent to the maximum absorbance peak, recovery yield (RY), surface morphology and conjugation efficiency.

When using a 5:3 gold:RA ratio (m/m) for the synthesis of AuNPs, the resultant core mean size was 88 nm, while using a 5:10 gold:RA ratio (m/m) resulted in AuNPs cores with much larger mean size (~315 nm; $p<0.001$).

When the AuNPs were coated with HAOA, resultant particle size increased. It is to note that this tendency to increase in size after coating was more pronounced in the formulation synthetized using the 5:3 gold:RA ratio (~40%, ns) than the 5:10 gold:RA ratio (~12%, ns). This difference in particle size increment after coating can be explained by the fact that the 5:10 AuNP core is much larger. Since the quantity of HAOA coating used in both formulations was the same, it resulted in a larger surface area to cover and therefore less quantity of HAOA was available per individual AuNP in the 5:10 AuNP, when compared to the 5:3 AuNP core. Moreover, the larger size increase might be a consequence of the high concentration of this compound in the HAOA coating in addition to the high molecular weight of Hyaluronic Acid

(~1.5-1.8 x 10^6 Da), but also. Similar size increases after HAOA coating were seen in the previous reported formulation for melanoma [58].

The formulation herein described is intended to be administered *in situ,* therefore not delivered into the systemic circulation, but instead to be locally taken up by phagocytic cells, and afterwards cleared by the reticuloendothelial system and the liver. On one hand, it has been described that phagocytic cells, including macrophages, neutrophils and dendritic cells, are able to uptake NPs with mean sizes up to 1 μm [184,185]. On the other hand, formulation clearance, both reticuloendothelial and hepatic, should occur only after activation of the formulations and conclusion the PTT session. Thus, it has been described that NPs size should be greater than 200 nm [184,185].

Having these size-related clearance aspects in consideration, the 5:10 AuNPs' core seems to be more adequate than both the 5:3 AuNPs and previously designed formulation for melanoma [58,161], since both of these cores are smaller and, even after coating with HAOA, remain smaller than 200 nm, these cores present a higher risk of entering systemic circulation by intravasation through the tumor leaky vasculature [184,185].

Still regarding the characterization of the AuNPs size, PdI of the 5:3 and 5:10 AuNPs was determined, allowing to assess the formulations size distribution.

More uninform AuNPs were observed with the 5:3 ratio, uncoated and coated. PdIs' up to 0.5 are deemed acceptable, according with the literature [186]. Moreover, although the 5:10 AuNPs core PdI was higher, it decreased following HAOA coating, which suggests that the coating contributes for monodispersion of the 5:10 AuNP's size. This was not the case for the 5:3 AuNPs, as its PdI remained approximately unchanged before and after the HAOA coating.

Moreover, the individual size distribution of NPs within a NP population should be minimal. Indeed, it is important for a formulation to be monodisperse, as this characteristic standardizes the formulation's properties, as well as it allows great predictability for the *in vitro* and *in vivo* NPs behavior [187–189]. For instance, cellular uptake of AuNPs is, like for other materials-based NPs, influenced by PdI; therefore, if the AuNPs population have an uniform size distribution, it is easier to predict the proportion and rate of NPs internalization, but if NPs present polydispersed size distribution, their cellular internalization will occur in an unpredictable random manner [190]. Furthermore, AuNPs biodistribution is also size-dependent and, consequently, monodisperse formulations accumulate more uniformly [191] and, therefore, in a more predictable fashion.

AuNP's size also seems to influence the SPR band/Abs_{max} of AuNPs. Indeed, as AuNP size increases, the SPR band seems to move towards the right end of the radiation spectrum, to

higher wavelengths [48]. Moreover, SPR band is also influenced by size polydispersity of the AuNPs population, with more uniform populations of AuNPs having a more defined peak of absorbance for a certain wavelength, unlike populations with higher PdIs, which absorb throughout a broader range of wavelengths [192]. This was the case of the results presented herein, with the smaller AuNPs (5:3) having a SPR band in the visible region of the light spectrum, and the larger AuNPs (5:10) having a SPR band in NIR wavelengths. The HAOA coating, used to increase biocompatibility (discussed below), is also expected to cause a shift of absorbance towards higher wavelengths, *i.e.*, to the right end of the light spectrum. This was reflected in the 5:10 AuNPs, as the SPR band shifted to 840 nm with the coating addition, whereas in the 5:3 AuNPs SPR band remained unchanged (see Table 5). Taking into consideration that it is of interest that the final formulation of AuNPs would absorb in the wavelength range of the previously mentioned biologic windows (700-980 nm and 1000-1400 nm), the SPR band presented by the 5:10 AuNPs seems to be more adequate. Furthermore, 5:10 AuNPs present an improved higher SPR band (840 nm) when compared to the previously reported formulation developed for melanoma (709 nm) [161]. This represents significant improvement, as the laser used for the activation of AuNPs emits at 808 nm.

In order to achieve fully functional AuNPs, selective for aplastic thyroid carcinoma, ligand(s) had be chosen for surface modification of the formulation. The formulation's targets were chosen by selecting membrane receptors known to be overexpressed in anaplastic thyroid carcinoma cells. Two target receptors were selected: epidermal growth factor receptor (EGFR) [122,123,126,193] and type I transferrin receptor (TfR1/CD71) [131,194,195]. In order to target those receptors, three ligands were selected for the surface functionalization: human EGF, the ligand for EGFR; lapatinib, an EGFR and HER-2 tyrosine kinase inhibitor [196]; and human HTf, the iron-bound form of the ligand (transferrin) for TfR1/CD71.

Formulations were characterized regarding its RY and surface morphology, and the efficiency of surface functionalization was determined by calculating the conjugation efficiency.

Surface morphology was assessed by TEM. It was clear that the 5:10 AuNPs' core presented a very well-define icosahedron shape. In fact, the novel (5:10) AuNP core was much more uniform than the previously described formulation, which was heterogenous [161] and more similar to the 5:3 AuNPs core. Regarding the functionalization of the 5:10 HAOA-coated AuNPs, there was no difference in shape before (HAOA-coated AuNPs) and after functionalization with either EGF or HTf, as the shape remained spherical and well defined. However, the shape changed after lapatinib functionalization, with both spherical and more

elongated lapatinib-functionalized HAOA-coated 5:10 AuNPs. The functionalization also induced a change in the HAOA-coated AuNPs size: the coated AuNPs size increased two-fold factor when functionalized with EGF in contrast to 1.1. to 1.4-fold when functionalized with HTf and lapatinib. Nevertheless, all functionalized formulations had sizes that met the criteria for ideal size previously discussed, *i.e.,* between 200 nm and 1 μm.

The efficiency of ligand conjugation to the HAOA-coated AuNPs was determined for EGF, HTf and lapatinib (ongoing quantification). Both EGF and HTf conjugated efficiently to the surface of the HAOA-coated AuNPs, with HTf having the highest conjugation efficiency. RY indicates the percentage of materials/reagents that formed AuNPs, and is a very important parameter for industrial scale level. All formulations presented an adequate RY, with 66.0 ± 0.9 % for EGF, 70.0 ± 3.4 % for HTf, and 86.2 ± 36.5 % for lapatinib, which will be important for industrial scale-up.

The relationship between AuNPs SPR band and how both HAOA coating and ligand-binding affects absorbance of the functionalized coated AuNPs is also important for formulation's efficacy and, therefore, matter for discussion. Due to the fact that the ligands EGF, HTf and lapatinib present maximum absorption at wavelengths in the UV range, the SPR band of the functionalized formulations shifted towards the left end of the light spectrum, when compared to the non-functionalized HAOA-coated AuNPs. Moreover, functionalizing the HAOA-coated AuNPs with lapatinib caused a more pronounced shift, resulting in a SPR band in the visible range of the light spectrum.

As mentioned, it is of interest to formulate AuNPs that absorb NIR wavelengths (650-950 nm) as these regions of the light spectrum have high photostability, they can go through an high deepness, low absorption and low damage by/to the surrounding healthy off-target tissues [56,197]. This characteristic is in favor of the 5:10 formulation. Due to the 5:10 ratio gold:RA (m/m) AuNPs having favorable size and SPR band, this was the selected formulation that was functionalized and used in the assays.

5.3 Safety, efficacy and selectivity in vitro assays

As mentioned earlier, the formulation must be biocompatible with healthy tissues, but must also be cytotoxic and selective for anaplastic thyroid carcinoma cells, upon activation by laser. For this purpose, safety, efficacy and selectivity were studied *in vitro* using two cell lines: HaCat, a human non-pathological epithelial cell line; and 8505C, a human anaplastic thyroid

carcinoma cell line. Biocompatibility was assessed by incubating HaCat cells with different concentrations of the several formulations for 24 h.

As expected, the uncoated AuNPs at a concentration of 80 μM, were cytotoxic for the healthy cells, which was resolved by adding the HAOA-coating, rendering the coated AuNPs nontoxic, *i.e.*, biocompatible. The HAOA-coating not only increases biocompatibility, as shown by our data, but also improves optical properties and allows more effective functionalization of the AuNPs' surface by adsorbing the ligands. According to ISO 10993-5:2009(E), formulations that result in a decrease of cellular viability greater than 30% are classified as cytotoxic [198]. Thus, according to ISO standards, all coated formulations tested, including both functionalized and not functionalized, were non-toxic and therefore biocompatible with HaCat cells at 20 and 80 μM concentration, as the maximum reduction in cell viability observed was only 17%. Also, our *in vitro* assays suggest that this formulation seems safer than the previously HAOA-coated AuNPs developed to treat melanoma [161]. Indeed, using the same concentration (80 μM) and the same cell line (HaCat), the previously reported melanoma-specific AuNPs) caused 25% reduction of cell viability [161], considerably higher than our HAOA-coated AuNPs reported herein, which further supports the safety of our anaplastic thyroid carcinoma-specific AuNPs.

The efficacy of the different formulations was studied by analysing cellular viability after incubation with the laser-activated and not-activated AuNPs, HAOA-coated AuNPs and functionalized HAOA-coated AuNPs. The cytotoxicity action of the laser was also addressed by irradiating non-treated cells with the laser used to activate the formulations, and no reduction in cell viability was seen. In addition to its *in vitro* safety, the laser system used to activate the formulations has shown to be very suitable and easily implementable for clinical applications, mainly due to its easy and intuitive manipulation, but also due to the device mobility. Regarding the formulations, it is to note that, when not activated, uncoated-AuNPs and HTf-functionalized HAOA-coated AuNPs were effective in reducing anaplastic thyroid carcinoma cells' viability to 61% and 34%, respectively. However, the cell viability was greatly reduced to 42% (AuNPs) and 22% (HTf-functionalized HAOA-coated AuNPs), when laser was used to activate the formulations. Thus, laser-induced activation of the formulations resulted in a significant decrease in cell viability, when compared with the non-activated formulation. According to ISO 10993-5:2009(E) the non-activated HAOA-coated AuNPs, EGF-functionalized HAOA-coated AuNPs and lapatinib-coated HAOA-coated AuNPs were not cytotoxic for anaplastic thyroid carcinoma cells, resulting in cell viabilities of 89%, 87% and 77%, respectively. Although activating HAOA-coated AuNPs and EGF-functionalized

HAOA-coated AuNPs resulted in significant cell viability decrease, when compared with the respective non-activated formulations, HAOA-coated AuNPs still had no cytotoxicity against the 8505C cells, according to ISO standards. Although EGF- and lapatinib-functionalized HAOA-coated AuNPs were cytotoxic against anaplastic thyroid carcinoma cells, both decreasing cell viability to 62% when activated, HTf-functionalized HAOA-coated AuNPs was the most effective formulation, with the highest toxicity against anaplastic thyroid carcinoma cells, when activated (cell viability of ~22%) and not activated (cell viability of ~34%), at 80 μM.

Therefore, these data suggest that surface functionalization of the HAOA-coated AuNPs is key to increase the cytotoxic action against the anaplastic thyroid carcinoma cell line, being that HTf-functionalized HAOA-coated AuNPs was the most effective formulation.

Selectivity was assessed by comparing cell viabilities of HaCat cells (nonpathological cells) and 8505C (anaplastic thyroid carcinoma cells), after being incubated for 24h with the different formulations, not activated by laser, at 20 and 80 μM. The formulation was considered to be selective for anaplastic thyroid carcinoma if the cell viability observed in 8505C was significantly lower than cell viability of HaCat.

For the 20 μM concentration, no formulation resulted in a significant decrease of 8505C cell viability when compared to HaCat. At 80 μM, two formulations significantly decreased cell viability: AuNPs; and HTf-functionalized HAOA-coated AuNPs. Although AuNPs seems to be selective and cytotoxic for anaplastic thyroid carcinoma cells, it failed to be biocompatible for healthy cells (HaCat) and thus, HTf-functionalized HAOA-coated AuNPs seem to be the most suitable formulation. This formulation was biocompatible with HaCat cells, demonstrating a very small decrease in viability of this cell line, and it was also the most effective against anaplastic thyroid carcinoma cells, both when activated and when not activated by laser. Our data suggest that HTf-functionalized HAOA-coated AuNPs is selective for the anaplastic thyroid carcinoma cells and, therefore, this was the selected formulation for the *in vivo* experiments that aimed to assess safety and biodistribution, discussed below.

5.4 Haemolytic activity assay

Although the final formulation is intended for intratumoural or *in situ* administration, there is still the possibility (probably low) that it could enter the blood stream through its clearance or by intravasation of the tumour vessels. Thus, the haemolytic activity was studied to test if the formulations (AuNPs, HAOA-coated AuNPs, and HTf-functionalized HAOA-coated

AuNPs) were safe. A wide range of concentrations were studied (0.04 to 80 μM) and all formulations, at all the tested concentrations, presented an haemolytic activity bellow 2%, which, according to the literature, is considered non-haemolytic [199]. Therefore, one can state that AuNPs, HAOA-coated AuNPs, and HTf-functionalized HAOA-coated AuNPs formulations are safe if in contact with blood. Moreover, comparison between the three formulations, suggested that the safest formulation is the HTf-functionalized HAOA-coated AuNPs, since for almost all concentrations, this was the formulation that presented the lowest haemolytic activity. Considering the low haemolytic activity achieved, confirmed that HTf-functionalized HAOA-coated AuNPs are safe for parental administration and/or in case it reaches the bloodstream or its cellular components, namely erythrocytes.

5.5 Safety and biodistribution in vivo assays

Biodistribution and safety assessments were separately carried out *in vivo* using HAOA-coated AuNPs and HTf-functionalized HAOA-coated AuNPs.

For the safety assessment, HAOA-coated AuNPs were administrated subcutaneously (s.c) to the thyroid neck region of mice. At most timepoints tested, the HAOA-coated AuNPs were still present in the s.c. adipocyte tissue, adjacent to the s.c. administration site, indicating that most AuNPs had yet to be cleared from this region. In fact, HAOA-coated AuNPs seem to trigger the presence of macrophages at around 24h, with cellular infiltrates with phagocyted AuNPs being observed. It has been described that although AuNPs are rapidly phagocyted after being administrated, polymeric coatings are associated with reduced phagocytosis [200]. Furthermore, when phagocyted or uptaken by human cells, AuNPs do not seem to be cytotoxic [201], as was also seen in the HaCat assays. This could explain why these infiltrates were only present at 24h, as the functionalization and coating are expected to dramatically change the biodistribution of the AuNPs in comparison to other AuNPs-only formulations, and this will be clarified when the results of the ICP-MS are analysed. Based on other studies, AuNPs biodistribution seems to be size-dependent and, with sizes greater than 200 nm, are not expected to cross the blood-brain barrier and tend to accumulate mainly in the liver but some accumulation is also seen in the lungs, spleen and kidneys [201,202]. However, there were no organ modifications that could indicate AuNPs-induced lesions and/or rapid clearance. Indeed, clearance was not significant before the 24h timepoint, which is of the outmost importance, since the aim is for the AuNPs to be cleared from the tumour site only after laser activation and PTT session are concluded.

For the biodistribution assay, HTf-functionalized HAOA-coated AuNPs and HAOA-coated AuNPs were administrated and tissue indexes were determined. The tissue indexes provide important information regarding chemically-induced changes to the analysed organs. Under physiological healthy circumstances, tissue indexes remain constant. However, increased tissue index might suggest an organ hypertrophy or congestion, whereas decreased tissue index may indicate that the organ may have undergone atrophy or any other degenerative changes [175,203].

HAOA-coated AuNPs caused a hepatomegaly 24 h post-administration. Moreover, HTf-functionalized HAOA-coated AuNPs administration also resulted in an increase of hepatic tissue index, both 4 h and 24 h after administration, although more pronounced at 24 h post-administration. The increase of liver's tissue index may be related with the higher expression of the TfR1/CD71 [204], which causes higher hepatic affinity for HTf-functionalized HAOA-coated AuNPs, thus leading to its accumulation in the liver. However, hepatic TfR1/CD71 expression does not fully explain the increased liver tissue index that resulted from HAOA-coated AuNPs administration. In fact, it has been described that when NPs' surface is impregnated with Tf, its liver accumulation is not dependent on Tf content and that most nanoformulations accumulate in the liver as part of their normal clearance and excretion processes [205,206]. Furthermore, since we found no histologic abnormalities were in the liver, one can infer that the increased liver tissue index is related to AuNPs hepatic accumulation, as part of their normal clearance process. Nevertheless, others have suggested that in tumours with high TfR1/CD71 expression, such as anaplastic thyroid carcinoma, Tf-funcionalized NPs tend to accumulate more in the tumour itself than in the liver, when compared to the not-functionalized counterpart [205]. This aspect still needs to be evaluated by comparing with the pending results and further testing using our HTf-functionalized HAOA-coated AuNPs must be conducted, which we aim to do in the future, using *in vivo* murine models of anaplastic thyroid carcinoma.

Biodistribution of AuNPs have been assessed by other groups. For instance, Bailly *et al*., described that AuNPs, after 24 h post intravenous administration, accumulated mainly in the kidneys, liver, spleen and tumour [173]. However, and in similarity to other AuNPs' properties, *in vivo* biodistribution seems to be size dependent, and although the AuNPs of the previous presented study accumulated in the kidneys, this accumulation is associated with smaller sized AuNPs and, as size of AuNPs increases, kidney accumulation decreases [207]. Taking these results together, the HTf-functionalized HAOA-coated AuNPs are deemed as safe for *in situ* administration *in vivo*.

With all these results in mind, the HTf-functionalized HAOA-coated (5:10) AuNPs gathers all the required characteristics for the design of an anaplastic thyroid carcinoma-specific AuNPs for NIR-PTT. Indeed, our functionalized coated NPs present a size between 200 nm and 1 μm, allowing it to be phagocyted by cells and pass hepatic clearance, as demonstrated *in vivo*; concerning size and shape, the AuNPs are monodisperse, allowing the predictability of the formulations *in vivo* behaviour, pharmacologic and physicochemical properties as well as how the AuNPs will interact with biologic entities such as cells; our NPs present spherical morphology, optimizing surface-area-to-volume ratio, and consequently cell internalization; their SPR band is within the NIR wavelengths, and more specifically in the 800s' nm, ensuring optimal activation by the laser emitting at 808 nm; they are safe and non-haemolytic, as tested *in vitro* and *in vivo*; and finally, our anaplastic thyroid carcinoma-specific AuNPs were selective and cytotoxic for anaplastic thyroid carcinoma, causing a very significative decrease in cell viability of an anaplastic thyroid carcinoma cell line, upon laser activation.

Although our data suggests that our HTf-functionalized HAOA-coated (5:10) AuNPs are safe, additional *in vivo* studies are required to confirm the safety of these anaplastic thyroid carcinoma-specific AuNPs after single and multiple dose. The correlation of *in vitro* and *in vivo* assays and its predictable value (transnationality) must be accurate analysed in a very near future

The project reported herein resulted in very exciting preliminary results of a formulation designed for NIR-PTT of a very lethal malignancy, anaplastic thyroid carcinoma. Taking solely these results into account, this formulation seems promising for a possible treatment, either as palliative treatment to improve patients quality of life by, for example, reducing tumour mass, as adjuvant therapy, to reduce the anaplastic thyroid carcinoma mass and allow it to be surgically resettable, or as monotherapy, that would completely ablate anaplastic thyroid carcinoma.

6. Conclusions and Future Perspectives

The work presented herein explored the feasibility of a new formulation of functionalized AuNPs, for photothermal therapy (PTT) of anaplastic thyroid carcinoma, one of the most lethal malignancies with no current viable treatment course. Several combinations of ligands and AuNP cores were tested. Although all functionalized formulations were deemed safe for a healthy epithelial cell line and selective for anaplastic thyroid carcinoma, the HTf-functionalized HAOA-coated (5:10) AuNPs was the one formulation that presented the best set of characteristics suitable to specifically target anaplastic thyroid carcinoma cells for PTT. Our preliminary *in vivo* studies also rendered this formulation as safe, with no abnormalities of the analysed organs were detected. However, some of the results of the biodistribution assay are still pending (*i.e.,* quantification of gold in organs and blood by ICP-MS), as only the tissue indexes (with no abnormalities) were determined; this obviously constitutes a caveat in our work and a future objective to pursuit.

Taking all the results reported into consideration, the innovative formulation developed by our group - the holo-Transferrin functionalized HAOA-coated AuNPs - was demonstrated to have all the desired physical characteristics and had very promising preliminary results regarding selectivity and efficacy *in vitro,* and *in vivo* and *in vitro* safety, for PTT to be used in anaplastic thyroid carcinoma.

In the future, there are still assays and assessments that should be conducted concerning the development of anaplastic thyroid carcinoma-specific AuNPs for PTT.

For instance, it would be interesting to determine how long it takes for the anaplastic thyroid carcinoma cell lines to uptake the AuNPs (core, coated and functionalized) and to assess the impact of the different formulation processes on this time period. Furthermore, regarding *in vitro* experiments, it is of great interest to determine the cell-death mechanism (*i.e.,* apoptosis or necrosis) behind the AuNP-induced loss of cellular viability. Furthermore, we also plan to test if the cells at a specific stage of the cell cycle are more susceptible to the AuNPs' action.

Concerning the future *in vivo* experiments, our group has established collaborations with veterinary hospitals, in order to test the efficacy of the HTf-functionalized HAOA-coated AuNPs for PTT in animals at advanced stages of anaplastic thyroid carcinoma, when all viable treatment options have failed, following a rational assessment of risk *versus* benefits by a multidisciplinary team and always ensuring the strict respect for both ethical requirements and Portuguese law.

Although this project still has plenty steps towards its completion, from these preliminary results it is clear that this is a very promising and interesting research line that must be continued.

7. References

[1] Rebelo A, Molpeceres J, Rijo P, Pinto Reis C. Pancreatic Cancer Therapy Review: From Classic Therapeutic Agents to Modern Nanotechnologies. Curr Drug Metab 2017;18(4):346–59.

[2] Mallick S, Choi JS. Liposomes: Versatile and Biocompatible Nanovesicles for Efficient Biomolecules Delivery. J Nanosci Nanotechnol 2014;14(1):755–65.

[3] Ramsden JJ. Nanotechnology for Health, Food, and Hygiene. Appl. Nanotechnol., Elsevier; 2018, p. 81–104.

[4] Hua S, Wu SY. Editorial: Advances and Challenges in Nanomedicine. Front Pharmacol 2018;9.

[5] Chang EH, Harford JB, Eaton MAW, Boisseau PM, Dube A, Hayeshi R, et al. Nanomedicine: Past, present and future – A global perspective. Biochem Biophys Res Commun 2015;468(3):511–7.

[6] Bosetti R, Jones SL. Cost–effectiveness of nanomedicine: estimating the real size of nano-costs. Nanomedicine 2019;14(11):1367–70.

[7] Rostami I, Rezvani H, Hu Z, Shahmoradian SH. Breakthroughs in medicine and bioimaging with up-conversion nanoparticles. Int J Nanomedicine 2019;Volume 14:7759–80.

[8] Chen S, Liang X-J. Nanobiotechnology and nanomedicine: small change brings big difference. Sci China Life Sci 2018;61(4):371–2.

[9] Misra R, Acharya S, Sahoo SK. Cancer nanotechnology: application of nanotechnology in cancer therapy. Drug Discov Today 2010;15(19–20):842–50.

[10] Din F ud, Aman W, Ullah I, Qureshi OS, Mustapha O, Shafique S, et al. Effective use of nanocarriers as drug delivery systems for the treatment of selected tumors. Int J Nanomedicine 2017;Volume 12:7291–309.

[11] Barenholz Y (Chezy). Doxil® — The first FDA-approved nano-drug: Lessons learned. J Control Release 2012;160(2):117–34.

[12] Weissig V, Pettinger T, Murdock N. Nanopharmaceuticals (part 1): products on the market. Int J Nanomedicine 2014;4357.

[13] Forssen EA. The design and development of DaunoXome® for solid tumor targeting in vivo. Adv Drug Deliv Rev 1997;24(2–3):133–50.

[14] Wang M, Thanou M. Targeting nanoparticles to cancer. Pharmacol Res 2010;62(2):90–9.

[15] Nguyen KT. Targeted Nanoparticles for Cancer Therapy: Promises and Challenges. J Nanomed Nanotechnol 2011;02(05).

[16] Chen G, Roy I, Yang C, Prasad PN. Nanochemistry and Nanomedicine for Nanoparticle-based Diagnostics and Therapy. Chem Rev 2016;116(5):2826–85.

[17] Aslan B, Ozpolat B, Sood AK, Lopez-Berestein G. Nanotechnology in cancer therapy. J Drug Target 2013;21(10):904–13.

[18] Oyelere A. Gold nanoparticles: From nanomedicine to nanosensing. Nanotechnol Sci Appl 2008;Volume 1:45–66.

[19] Fay F, Scott CJ. Antibody-targeted nanoparticles for cancer therapy. Immunotherapy 2011;3(3):381–94.

[20] Alexis F, Rhee J-W, Richie JP, Radovic-Moreno AF, Langer R, Farokhzad OC. New frontiers in nanotechnology for cancer treatment. Urol Oncol Semin Orig Investig 2008;26(1):74–85.

[21] Schaaf MB, Garg AD, Agostinis P. Defining the role of the tumor vasculature in antitumor immunity and immunotherapy. Cell Death Dis 2018;9(2):115.

[22] Ashraf S, Pelaz B, del Pino P, Carril M, Escudero A, Parak WJ, et al. Gold-Based Nanomaterials for Applications in Nanomedicine, 2016, p. 169–202.

[23] Carabineiro S. Applications of Gold Nanoparticles in Nanomedicine: Recent Advances in Vaccines. Molecules 2017;22(5):857.

[24] Prasad R, Jain NK, Yadav AS, Chauhan DS, Devrukhkar J, Kumawat MK, et al. Liposomal nanotheranostics for multimode targeted in vivo bioimaging and near-infrared light mediated cancer therapy. Commun Biol 2020;3(1):284.
[25] Guo J, Rahme K, He Y, Li L-L, Holmes J, O'Driscoll C. Gold nanoparticles enlighten the future of cancer theranostics. Int J Nanomedicine 2017;Volume 12:6131–52.
[26] Almeida JPM, Figueroa ER, Drezek RA. Gold nanoparticle mediated cancer immunotherapy. Nanomedicine Nanotechnology, Biol Med 2014;10(3):503–14.
[27] Haume K, Rosa S, Grellet S, Śmiałek MA, Butterworth KT, Solov'yov A V., et al. Gold nanoparticles for cancer radiotherapy: a review. Cancer Nanotechnol 2016;7(1):8.
[28] Zhang X. Gold Nanoparticles: Recent Advances in the Biomedical Applications. Cell Biochem Biophys 2015;72(3):771–5.
[29] Kim C, Ghosh P, Rotello VM. Multimodal drug delivery using gold nanoparticles. Nanoscale 2009;1(1):61.
[30] Ajnai G, Chiu A, Kan T, Cheng C-C, Tsai T-H, Chang J. Trends of Gold Nanoparticle-based Drug Delivery System in Cancer Therapy. J Exp Clin Med 2014;6(6):172–8.
[31] Ma P, Mumper RJ. Anthracycline nano-delivery systems to overcome multiple drug resistance: A comprehensive review. Nano Today 2013;8(3):313–31.
[32] Dreaden EC, Austin LA, Mackey MA, El-Sayed MA. Size matters: gold nanoparticles in targeted cancer drug delivery. Ther Deliv 2012;3(4):457–78.
[33] Meng CSW, Pan Y, Zhao X. Epirubicin-gold nanoparticles suppress hepatocellular carcinoma xenograft growth in nude mice. J Biomed Res 2015;
[34] Her S, Jaffray DA, Allen C. Gold nanoparticles for applications in cancer radiotherapy: Mechanisms and recent advancements. Adv Drug Deliv Rev 2017;109:84–101.
[35] Lucky SS, Soo KC, Zhang Y. Nanoparticles in Photodynamic Therapy. Chem Rev 2015;115(4):1990–2042.
[36] Huang X, El-Sayed MA. Plasmonic photo-thermal therapy (PPTT). Alexandria J Med 2011;47(1):1–9.
[37] Shibu ES, Hamada M, Murase N, Biju V. Nanomaterials formulations for photothermal and photodynamic therapy of cancer. J Photochem Photobiol C Photochem Rev 2013;15:53–72.
[38] Stuchinskaya T, Moreno M, Cook MJ, Edwards DR, Russell DA. Targeted photodynamic therapy of breast cancer cells using antibody–phthalocyanine–gold nanoparticle conjugates. Photochem Photobiol Sci 2011;10(5):822.
[39] Meyers JD, Cheng Y, Broome A-M, Agnes RS, Schluchter MD, Margevicius S, et al. Peptide-Targeted Gold Nanoparticles for Photodynamic Therapy of Brain Cancer. Part Part Syst Charact 2015;32(4):448–57.
[40] García Calavia P, Chambrier I, Cook MJ, Haines AH, Field RA, Russell DA. Targeted photodynamic therapy of breast cancer cells using lactose-phthalocyanine functionalized gold nanoparticles. J Colloid Interface Sci 2018;512:249–59.
[41] Zou L, Wang H, He B, Zeng L, Tan T, Cao H, et al. Current Approaches of Photothermal Therapy in Treating Cancer Metastasis with Nanotherapeutics. Theranostics 2016;6(6):762–72.
[42] Huang X, Jain PK, El-Sayed IH, El-Sayed MA. Plasmonic photothermal therapy (PPTT) using gold nanoparticles. Lasers Med Sci 2008;23(3):217–28.
[43] Xu L, Cheng L, Wang C, Peng R, Liu Z. Conjugated polymers for photothermal therapy of cancer. Polym Chem 2014;5(5):1573–80.
[44] CABRAL RM, BAPTISTA P V. THE CHEMISTRY AND BIOLOGY OF GOLD NANOPARTICLE-MEDIATED PHOTOTHERMAL THERAPY: PROMISES AND CHALLENGES. Nano Life 2013;03(03):1330001.
[45] Jaque D, Martínez Maestro L, del Rosal B, Haro-Gonzalez P, Benayas A, Plaza JL, et al.

Nanoparticles for photothermal therapies. Nanoscale 2014;6(16):9494–530.
[46] Beik J, Abed Z, Ghoreishi FS, Hosseini-Nami S, Mehrzadi S, Shakeri-Zadeh A, et al. Nanotechnology in hyperthermia cancer therapy: From fundamental principles to advanced applications. J Control Release 2016;235:205–21.
[47] Pejjai B, Reddivari M, Kotte TRR. Phase controllable synthesis of CuS nanoparticles by chemical co-precipitation method: Effect of copper precursors on the properties of CuS. Mater Chem Phys 2020;239:122030.
[48] Vines JB, Yoon J-H, Ryu N-E, Lim D-J, Park H. Gold Nanoparticles for Photothermal Cancer Therapy. Front Chem 2019;7.
[49] Wang J, Qiu J. A review of organic nanomaterials in photothermal cancer therapy. Cancer Res Front 2016;2(1):67–84.
[50] Riley RS, Day ES. Gold nanoparticle-mediated photothermal therapy: applications and opportunities for multimodal cancer treatment. Wiley Interdiscip Rev Nanomedicine Nanobiotechnology 2017;9(4):e1449.
[51] Hwang S, Nam J, Jung S, Song J, Doh H, Kim S. Gold nanoparticle-mediated photothermal therapy: current status and future perspective. Nanomedicine 2014;9(13):2003–22.
[52] Huang X, El-Sayed MA. Gold nanoparticles: Optical properties and implementations in cancer diagnosis and photothermal therapy. J Adv Res 2010;1(1):13–28.
[53] Mendes R, Pedrosa P, Lima JC, Fernandes AR, Baptista P V. Photothermal enhancement of chemotherapy in breast cancer by visible irradiation of Gold Nanoparticles. Sci Rep 2017;7(1):10872.
[54] Chung US, Kim J-H, Kim B, Kim E, Jang W-D, Koh W-G. Dendrimer porphyrin-coated gold nanoshells for the synergistic combination of photodynamic and photothermal therapy. Chem Commun 2016;52(6):1258–61.
[55] Wu P, Gao Y, Zhang H, Cai C. Aptamer-Guided Silver–Gold Bimetallic Nanostructures with Highly Active Surface-Enhanced Raman Scattering for Specific Detection and Near-Infrared Photothermal Therapy of Human Breast Cancer Cells. Anal Chem 2012;84(18):7692–9.
[56] Zhou J, Lu Z, Zhu X, Wang X, Liao Y, Ma Z, et al. NIR photothermal therapy using polyaniline nanoparticles. Biomaterials 2013;34(37):9584–92.
[57] Yang W, Liang H, Ma S, Wang D, Huang J. Gold nanoparticle based photothermal therapy: Development and application for effective cancer treatment. Sustain Mater Technol 2019;22:e00109.
[58] Silva CO, Petersen SB, Reis CP, Rijo P, Molpeceres J, Fernandes AS, et al. EGF Functionalized Polymer-Coated Gold Nanoparticles Promote EGF Photostability and EGFR Internalization for Photothermal Therapy. PLoS One 2016;11(10):e0165419.
[59] Singh SP, Alvi SB, Pemmaraju DB, Singh AD, Manda SV, Srivastava R, et al. NIR triggered liposome gold nanoparticles entrapping curcumin as in situ adjuvant for photothermal treatment of skin cancer. Int J Biol Macromol 2018;110:375–82.
[60] Noh MS, Lee S, Kang H, Yang J-K, Lee H, Hwang D, et al. Target-specific near-IR induced drug release and photothermal therapy with accumulated Au/Ag hollow nanoshells on pulmonary cancer cell membranes. Biomaterials 2015;45:81–92.
[61] Zhang M, Kim HS, Jin T, Moon WK. Near-infrared photothermal therapy using EGFR-targeted gold nanoparticles increases autophagic cell death in breast cancer. J Photochem Photobiol B Biol 2017;170:58–64.
[62] Arnida, Malugin A, Ghandehari H. Cellular uptake and toxicity of gold nanoparticles in prostate cancer cells: a comparative study of rods and spheres. J Appl Toxicol 2009;n/a-n/a.
[63] Salem DS, Sliem MA, El-Sesy M, Shouman SA, Badr Y. Improved chemo-photothermal therapy of hepatocellular carcinoma using chitosan-coated gold nanoparticles. J Photochem

Photobiol B Biol 2018;182:92–9.
[64] Goodrich GP, Bao L, Gill-Sharp K, Sang KL, Wang J, Payne JD. Photothermal therapy in a murine colon cancer model using near-infrared absorbing gold nanorods. J Biomed Opt 2010;15(1):018001.
[65] Yeh Y-C, Creran B, Rotello VM. Gold nanoparticles: preparation, properties, and applications in bionanotechnology. Nanoscale 2012;4(6):1871–80.
[66] Vigderman L, Zubarev ER. Therapeutic platforms based on gold nanoparticles and their covalent conjugates with drug molecules. Adv Drug Deliv Rev 2013;65(5):663–76.
[67] Rayavarapu RG, Petersen W, Hartsuiker L, Chin P, Janssen H, van Leeuwen FWB, et al. In vitro toxicity studies of polymer-coated gold nanorods. Nanotechnology 2010;21(14):145101.
[68] Muddineti OS, Ghosh B, Biswas S. Current trends in using polymer coated gold nanoparticles for cancer therapy. Int J Pharm 2015;484(1–2):252–67.
[69] AL-Jawad SMH, Taha AA, Al-Halbosiy MMF, AL-Barram LFA. Synthesis and characterization of small-sized gold nanoparticles coated by bovine serum albumin (BSA) for cancer photothermal therapy. Photodiagnosis Photodyn Ther 2018;21:201–10.
[70] Ahmad R, Fu J, He N, Li S. Advanced Gold Nanomaterials for Photothermal Therapy of Cancer. J Nanosci Nanotechnol 2016;16(1):67–80.
[71] Mallick S, Sun I-C, Kim K, Yi DK. Silica Coated Gold Nanorods for Imaging and Photo-Thermal Therapy of Cancer Cells. J Nanosci Nanotechnol 2013;13(5):3223–9.
[72] An SS, Kang JH, Ko YT. Lipid-coated gold nanocomposites for enhanced cancer therapy. Int J Nanomedicine 2015;33.
[73] Stathatos N. Anatomy and Physiology of the Thyroid Gland. Thyroid Cancer, Totowa, NJ: Humana Press; 2006, p. 3–7.
[74] Stathatos N. Thyroid Physiology. Med Clin North Am 2012;96(2):165–73.
[75] Rousset B, Dupuy C, Miot F, Dumont J. Chapter 2 Thyroid Hormone Synthesis And Secretion. 2000.
[76] Opitz R, Schmidt F, Braunbeck T, Wuertz S, Kloas W. Perchlorate and ethylenethiourea induce different histological and molecular alterations in a non-mammalian vertebrate model of thyroid goitrogenesis. Mol Cell Endocrinol 2009;298(1–2):101–14.
[77] Jugan M-L, Levi Y, Blondeau J-P. Endocrine disruptors and thyroid hormone physiology. Biochem Pharmacol 2010;79(7):939–47.
[78] Khan YS, Farhana A. Histology, Thyroid Gland. 2020.
[79] Gimm O. Thyroid cancer. Cancer Lett 2001;163(2):143–56.
[80] Kitahara CM, Sosa JA. The changing incidence of thyroid cancer. Nat Rev Endocrinol 2016;12(11):646–53.
[81] Nikiforova MN, Nikiforov YE. Molecular genetics of thyroid cancer: implications for diagnosis, treatment and prognosis. Expert Rev Mol Diagn 2008;8(1):83–95.
[82] Lin R-Y. Thyroid cancer stem cells. Nat Rev Endocrinol 2011;7(10):609–16.
[83] Kondo T, Ezzat S, Asa SL. Pathogenetic mechanisms in thyroid follicular-cell neoplasia. Nat Rev Cancer 2006;6(4):292–306.
[84] Soares P, Lima J, Preto A, Castro P, Vinagre J, Celestino R, et al. Genetic Alterations in Poorly Differentiated and Undifferentiated Thyroid Carcinomas. Curr Genomics 2011;12(8):609–17.
[85] Nguyen QT, Lee EJ, Huang MG, Park YI, Khullar A, Plodkowski RA. Diagnosis and treatment of patients with thyroid cancer. Am Heal Drug Benefits 2015;8(1):30–40.
[86] D'Avanzo A, Treseler P, Ituarte PHG, Wong M, Streja L, Greenspan FS, et al. Follicular thyroid carcinoma: Histology and prognosis. Cancer 2004;100(6):1123–9.
[87] Leboulleux S, Baudin E, Travagli J-P, Schlumberger M. Medullary thyroid carcinoma. Clin Endocrinol (Oxf) 2004;61(3):299–310.

[88] Nosé V. Familial Non-Medullary Thyroid Carcinoma: An Update. Endocr Pathol 2008;19(4):226–40.
[89] Robenshtok E, Tzvetov G, Grozinsky-Glasberg S, Shraga-Slutzky I, Weinstein R, Lazar L, et al. Clinical Characteristics and Outcome of Familial Nonmedullary Thyroid Cancer: A Retrospective Controlled Study. Thyroid 2011;21(1):43–8.
[90] Kebebew E, Greenspan FS, Clark OH, Woeber KA, McMillan A. Anaplastic thyroid carcinoma. Cancer 2005;103(7):1330–5.
[91] Wiseman SM, Loree TR, Rigual NR, Hicks WL, Douglas WG, Anderson GR, et al. Anaplastic transformation of thyroid cancer: Review of clinical, pathologic, and molecular evidence provides new insights into disease biology and future therapy. Head Neck 2003;25(8):662–70.
[92] Lang BH-H, Lo C-Y. Surgical Options in Undifferentiated Thyroid Carcinoma. World J Surg 2007;31(5):969–77.
[93] Liu T-R, Xiao Z-W, Xu H-N, Long Z, Wei F-Q, Zhuang S-M, et al. Treatment and Prognosis of Anaplastic Thyroid Carcinoma: A Clinical Study of 50 Cases. PLoS One 2016;11(10):e0164840.
[94] DeLellis RA. Pathology and genetics of thyroid carcinoma. J Surg Oncol 2006;94(8):662–9.
[95] Soares P, Trovisco V, Rocha A, Feij□o T, Rebocho A, Fonseca E, et al. BRAF mutations typical of papillary thyroid carcinoma are more frequently detected in undifferentiated than in insular and insular-like poorly differentiated carcinomas. Virchows Arch 2004;444(6).
[96] Nagaiah G, Hossain A, Mooney CJ, Parmentier J, Remick SC. Anaplastic Thyroid Cancer: A Review of Epidemiology, Pathogenesis, and Treatment. J Oncol 2011;2011:1–13.
[97] Green LD, Mack L, Pasieka JL. Anaplastic thyroid cancer and primary thyroid lymphoma: A review of these rare thyroid malignancies. J Surg Oncol 2006;94(8):725–36.
[98] Tiedje V, Stuschke M, Weber F, Dralle H, Moss L, Führer D. Anaplastic thyroid carcinoma: review of treatment protocols. Endocr Relat Cancer 2018;25(3):R153–61.
[99] Liu Y, Su L, Xiao H. Review of Factors Related to the Thyroid Cancer Epidemic. Int J Endocrinol 2017;2017:1–9.
[100] Khairy G. Anaplastic transformation of differentiated thyroid carcinoma. Int J Health Sci (Qassim) 2009;3(1):93–6.
[101] Dackiw APB. Anaplastic Thyroid Cancer, 2010, p. 75–84.
[102] Zivaljevic V, Tausanovic K, Paunovic I, Diklic A, Kalezic N, Zoric G, et al. Age as a Prognostic Factor in Anaplastic Thyroid Cancer. Int J Endocrinol 2014;2014:1–5.
[103] Tuttle RM, Ball DW, Byrd D, Dilawari RA, Doherty GM, Duh Q-Y, et al. Thyroid Carcinoma. J Natl Compr Cancer Netw 2010;8(11):1228–74.
[104] Shah JP. Thyroid carcinoma: epidemiology, histology, and diagnosis. Clin Adv Hematol Oncol 2015;13(4 Suppl 4):3–6.
[105] Filetti S, Durante C, Hartl D, Leboulleux S, Locati LD, Newbold K, et al. Thyroid cancer: ESMO Clinical Practice Guidelines for diagnosis, treatment and follow-up. Ann Oncol 2019;30(12):1856–83.
[106] Cady B. Staging in thyroid carcinoma. Cancer 1998;83(5):844–7.
[107] Tahara M, Kiyota N, Yamazaki T, Chayahara N, Nakano K, Inagaki L, et al. Lenvatinib for Anaplastic Thyroid Cancer. Front Oncol 2017;7.
[108] Ranganath R, Shah MA, Shah AR. Anaplastic thyroid cancer. Curr Opin Endocrinol Diabetes Obes 2015;22(5):387–91.
[109] Cabanillas ME, McFadden DG, Durante C. Thyroid cancer. Lancet 2016;388(10061):2783–95.
[110] Wein RO, Weber RS. Anaplastic thyroid carcinoma: palliation or treatment? Curr Opin Otolaryngol Head Neck Surg 2011;19(2):113–8.
[111] Are C, Shaha AR. Anaplastic Thyroid Carcinoma: Biology, Pathogenesis, Prognostic Factors,

and Treatment Approaches. Ann Surg Oncol 2006;13(4):453–64.
[112] Neff RL, Farrar WB, Kloos RT, Burman KD. Anaplastic Thyroid Cancer. Endocrinol Metab Clin North Am 2008;37(2):525–38.
[113] Nikiforov YE. Genetic Alterations Involved in the Transition from Well-Differentiated to Poorly Differentiated and Anaplastic Thyroid Carcinomas. Endocr Pathol 2004;15(4):319–28.
[114] Santarpia L, El-Naggar AK, Cote GJ, Myers JN, Sherman SI. Phosphatidylinositol 3-Kinase/Akt and Ras/Raf-Mitogen-Activated Protein Kinase Pathway Mutations in Anaplastic Thyroid Cancer. J Clin Endocrinol Metab 2008;93(1):278–84.
[115] Wang H-M, Huang Y-W, Huang J-S, Wang C-H, Kok VC, Hung C-M, et al. Anaplastic Carcinoma of the Thyroid Arising More Often from Follicular Carcinoma than Papillary Carcinoma. Ann Surg Oncol 2007;14(10):3011–8.
[116] Ragazzi M, Ciarrocchi A, Sancisi V, Gandolfi G, Bisagni A, Piana S. Update on Anaplastic Thyroid Carcinoma: Morphological, Molecular, and Genetic Features of the Most Aggressive Thyroid Cancer. Int J Endocrinol 2014;2014:1–13.
[117] Salvatore G, Nappi TC, Salerno P, Jiang Y, Garbi C, Ugolini C, et al. A Cell Proliferation and Chromosomal Instability Signature in Anaplastic Thyroid Carcinoma. Cancer Res 2007;67(21):10148–58.
[118] Quiros RM, Ding HG, Gattuso P, Prinz RA, Xu X. Evidence that one subset of anaplastic thyroid carcinomas are derived from papillary carcinomas due toBRAF andp53 mutations. Cancer 2005;103(11):2261–8.
[119] Antonelli A, Fallahi P, Ferrari SM, Carpi A, Berti P, Materazzi G, et al. Dedifferentiated thyroid cancer: A therapeutic challenge. Biomed Pharmacother 2008;62(8):559–63.
[120] Fisher KE, Jani JC, Fisher SB, Foulks C, Hill CE, Weber CJ, et al. Epidermal growth factor receptor overexpression is a marker for adverse pathologic features in papillary thyroid carcinoma. J Surg Res 2013;185(1):217–24.
[121] Landriscina M, Pannone G, Piscazzi A, Toti P, Fabiano A, Tortorella S, et al. Epidermal Growth Factor Receptor 1 Expression Is Upregulated in Undifferentiated Thyroid Carcinomas in Humans. Thyroid 2011;21(11):1227–34.
[122] Elliott DD, Sherman SI, Busaidy NL, Williams MD, Santarpia L, Clayman GL, et al. Growth factor receptors expression in anaplastic thyroid carcinoma: potential markers for therapeutic stratification. Hum Pathol 2008;39(1):15–20.
[123] Lee DH, Lee GK, Kong S -y., Kook MC, Yang SK, Park SY, et al. Epidermal growth factor receptor status in anaplastic thyroid carcinoma. J Clin Pathol 2006;60(8):881–4.
[124] O'Neill JP, Power D, Condron C, Bouchier-Hayes D, Walsh M. Anaplastic thyroid cancer, tumorigenesis and therapy. Ir J Med Sci 2010;179(1):9–15.
[125] Yarden Y. The EGFR family and its ligands in human cancer. Eur J Cancer 2001;37:3–8.
[126] Schiff BA. Epidermal Growth Factor Receptor (EGFR) Is Overexpressed in Anaplastic Thyroid Cancer, and the EGFR Inhibitor Gefitinib Inhibits the Growth of Anaplastic Thyroid Cancer. Clin Cancer Res 2004;10(24):8594–602.
[127] Nicholson R., Gee JM., Harper M. EGFR and cancer prognosis. Eur J Cancer 2001;37:9–15.
[128] Bergström JD, Westermark B, Heldin N-E. Epidermal Growth Factor Receptor Signaling Activates Met in Human Anaplastic Thyroid Carcinoma Cells. Exp Cell Res 2000;259(1):293–9.
[129] Knauf JA. Does the Epidermal Growth Factor Receptor Play a Role in the Progression of Thyroid Cancer? Thyroid 2011;21(11):1171–4.
[130] Xing M. Molecular pathogenesis and mechanisms of thyroid cancer. Nat Rev Cancer 2013;13(3):184–99.
[131] Parenti R, Salvatorelli L, Magro G. Anaplastic Thyroid Carcinoma: Current Treatments and

Potential New Therapeutic Options with Emphasis on TfR1/CD71. Int J Endocrinol 2014;2014:1–11.
[132] Shen Y, Li X, Dong D, Zhang B, Xue Y, Shang P. Transferrin receptor 1 in cancer: a new sight for cancer therapy. Am J Cancer Res 2018;8(6):916–31.
[133] Paschke R, Lincke T, Müller SP, Kreissl MC, Dralle H, Fassnacht M. The Treatment of Well-Differentiated Thyroid Carcinoma. Dtsch Aerzteblatt Online 2015;
[134] Akaishi J, Sugino K, Kitagawa W, Nagahama M, Kameyama K, Shimizu K, et al. Prognostic Factors and Treatment Outcomes of 100 Cases of Anaplastic Thyroid Carcinoma. Thyroid 2011;21(11):1183–9.
[135] Shaha AR. Airway Management in Anaplastic Thyroid Carcinoma. Laryngoscope 2008;118(7):1195–8.
[136] Huang L-Y, Lee Y-L, Chou P, Chiu W-Y, Chu D. Thyroid Fine-Needle Aspiration Biopsy and Thyroid Cancer Diagnosis: A Nationwide Population-Based Study. PLoS One 2015;10(5):e0127354.
[137] Lewinski A, Ferenc T, Sporny S, Jarzab B. Thyroid carcinoma: diagnostic and therapeutic approach; genetic background (review). Endocr Regul 2000;34(2):99–113.
[138] Sherman SI. Thyroid carcinoma. Lancet 2003;361(9356):501–11.
[139] Giuffrida D, Gharib H. Anaplastic thyroid carcinoma: Current diagnosis and treatment*. Ann Oncol 2000;11(9):1083–9.
[140] Lee SL. Complications of Radioactive Iodine Treatment of Thyroid Carcinoma. J Natl Compr Cancer Netw 2010;8(11):1277–87.
[141] Biondi B, Filetti S, Schlumberger M. Thyroid-hormone therapy and thyroid cancer: a reassessment. Nat Clin Pract Endocrinol Metab 2005;1(1):32–40.
[142] Ross DS. Radioiodine Therapy for Hyperthyroidism. N Engl J Med 2011;364(6):542–50.
[143] Schlumberger M, Brose M, Elisei R, Leboulleux S, Luster M, Pitoia F, et al. Definition and management of radioactive iodine-refractory differentiated thyroid cancer. Lancet Diabetes Endocrinol 2014;2(5):356–8.
[144] Jonklaas J, Sarlis NJ, Litofsky D, Ain KB, Bigos ST, Brierley JD, et al. Outcomes of Patients with Differentiated Thyroid Carcinoma Following Initial Therapy. Thyroid 2006;16(12):1229–42.
[145] Sawka AM, Thephamongkhol K, Brouwers M, Thabane L, Browman G, Gerstein HC. A Systematic Review and Metaanalysis of the Effectiveness of Radioactive Iodine Remnant Ablation for Well-Differentiated Thyroid Cancer. J Clin Endocrinol Metab 2004;89(8):3668–76.
[146] Brabant G. Thyrotropin Suppressive Therapy in Thyroid Carcinoma: What Are the Targets? J Clin Endocrinol Metab 2008;93(4):1167–9.
[147] McGriff NJ, Csako G, Gourgiotis L, Guthrie LC, Pucino F, Sarlis NJ. Effects of thyroid hormone suppression therapy on adverse clinical outcomes in thyroid cancer. Ann Med 2002;34(7):554–64.
[148] Sherman SI. Cytotoxic Chemotherapy for Differentiated Thyroid Carcinoma. Clin Oncol 2010;22(6):464–8.
[149] Busaidy NL, Cabanillas ME. Differentiated Thyroid Cancer: Management of Patients with Radioiodine Nonresponsive Disease. J Thyroid Res 2012;2012:1–12.
[150] Kloos RT. Protecting Thyroid Cancer Patients from Untoward Effects of Radioactive Iodine Treatment. Thyroid 2009;19(9):925–8.
[151] Pacini F, Castagna MG, Cipri C, Schlumberger M. Medullary Thyroid Carcinoma. Clin Oncol 2010;22(6):475–85.
[152] Harada T, Nishikawa Y, Suzuki T, Ito K, Baba S. Bleomycin treatment for cancer of the thyroid.

Am J Surg 1971;122(1):53–7.
[153] Liebner DA, Haraldsdottir S, Shah MH. Chemotherapy of Thyroid Cancer: General Principles. Thyroid Cancer, New York, NY: Springer New York; 2016, p. 717–21.
[154] Lim SW. Targeted Therapy of Thyroid Cancer, 2012, p. 301–15.
[155] Shimaoka K, Schoenfeld DA, Dewys WD, Creech RH, Deconti R. A randomized trial of doxorubicin versus doxorubicin plus cisplatin in patients with advanced thyroid carcinoma. Cancer 1985;56(9):2155–60.
[156] Smallridge RC, Ain KB, Asa SL, Bible KC, Brierley JD, Burman KD, et al. American Thyroid Association Guidelines for Management of Patients with Anaplastic Thyroid Cancer. Thyroid 2012;22(11):1104–39.
[157] Molinaro E, Romei C, Biagini A, Sabini E, Agate L, Mazzeo S, et al. Anaplastic thyroid carcinoma: from clinicopathology to genetics and advanced therapies. Nat Rev Endocrinol 2017;13(11):644–60.
[158] Smallridge RC, Copland JA. Anaplastic Thyroid Carcinoma: Pathogenesis and Emerging Therapies. Clin Oncol 2010;22(6):486–97.
[159] Haghpanah V, Fallah P, Naderi M, Tavakoli R, Soleimani M, Larijani B. Cancer stem-like cell behavior in anaplastic thyroid cancer: A challenging dilemma. Life Sci 2016;146:34–9.
[160] Zhou M, Chen Y, Adachi M, Wen X, Erwin B, Mawlawi O, et al. Single agent nanoparticle for radiotherapy and radio-photothermal therapy in anaplastic thyroid cancer. Biomaterials 2015;57:41–9.
[161] Silva CO, Rijo P, Molpeceres J, Ascensão L, Roberto A, Fernandes AS, et al. Bioproduction of gold nanoparticles for photothermal therapy. Ther Deliv 2016;7(5):287–304.
[162] Saini S, Tulla K, Maker A V., Burman KD, Prabhakar BS. Therapeutic advances in anaplastic thyroid cancer: a current perspective. Mol Cancer 2018;17(1):154.
[163] Smallridge RC, Marlow LA, Copland JA. Anaplastic thyroid cancer: molecular pathogenesis and emerging therapies. Endocr Relat Cancer 2009;16(1):17–44.
[164] Rosove MH, Peddi PF, Glaspy JA. BRAF V600E Inhibition in Anaplastic Thyroid Cancer. N Engl J Med 2013;368(7):684–5.
[165] Subbiah V, Kreitman RJ, Wainberg ZA, Cho JY, Schellens JHM, Soria JC, et al. Dabrafenib and Trametinib Treatment in Patients With Locally Advanced or Metastatic BRAF V600–Mutant Anaplastic Thyroid Cancer. J Clin Oncol 2018;36(1):7–13.
[166] Lim SM, Chang H, Yoon MJ, Hong YK, Kim H, Chung WY, et al. A multicenter, phase II trial of everolimus in locally advanced or metastatic thyroid cancer of all histologic subtypes. Ann Oncol 2013;24(12):3089–94.
[167] Grande E, Capdevila J, Díez JJ, Longo F, Carrato A. A significant response to sunitinib in a patient with anaplastic thyroid carcinoma. J Res Med Sci 2013;18(7):623–5.
[168] Ha HT, Lee JS, Urba S, Koenig RJ, Sisson J, Giordano T, et al. A Phase II Study of Imatinib in Patients with Advanced Anaplastic Thyroid Cancer. Thyroid 2010;20(9):975–80.
[169] Krähn G, Leiter U, Kaskel P, Udart M, Utikal J, Bezold G, et al. Coexpression patterns of EGFR, HER2, HER3 and HER4 in non-melanoma skin cancer. Eur J Cancer 2001;37(2):251–9.
[170] Saadat E. Development and Validation of Rapid RP-HPLC-DAD Analysis Method for Simultaneous Quantitation of Paclitaxel and Lapatinib in Polymeric Micelle Formulation. Sci Pharm 2016;84(2):333–45.
[171] Mota AH, Andrade JM, Rodrigues MJ, Custódio L, Bronze MR, Duarte N, et al. Synchronous insight of in vitro and in vivo biological activities of Sambucus nigra L. extracts for industrial uses. Ind Crops Prod 2020;154:112709.
[172] von Maltzahn G, Park J-H, Agrawal A, Bandaru NK, Das SK, Sailor MJ, et al. Computationally Guided Photothermal Tumor Therapy Using Long-Circulating Gold Nanorod Antennas. Cancer

Res 2009;69(9):3892–900.
[173] Bailly A-L, Correard F, Popov A, Tselikov G, Chaspoul F, Appay R, et al. In vivo evaluation of safety, biodistribution and pharmacokinetics of laser-synthesized gold nanoparticles. Sci Rep 2019;9(1):12890.
[174] Xu J, Yu M, Peng C, Carter P, Tian J, Ning X, et al. Dose Dependencies and Biocompatibility of Renal Clearable Gold Nanoparticles: From Mice to Non-human Primates. Angew Chemie Int Ed 2018;57(1):266–71.
[175] Pinho JO, Amaral JD, Castro RE, Rodrigues CM, Casini A, Soveral G, et al. Copper complex nanoformulations featuring highly promising therapeutic potential in murine melanoma models. Nanomedicine 2019;14(7):835–50.
[176] Amaral M, Afonso RA, Gaspar MM, Reis CP. Anaplastic thyroid cancer: How far can we go? EXCLI J 2020;19:800–12.
[177] Chaloupka K, Malam Y, Seifalian AM. Nanosilver as a new generation of nanoproduct in biomedical applications. Trends Biotechnol 2010;28(11):580–8.
[178] Biterge-Süt B, Canpolat E. Evaluation of Gold Nanoparticles in Terms of Their Use in Biomedical Applications. Turkish J Agric - Food Sci Technol 2019;7(10):1694.
[179] El Halabi I, Bejjany R, Nasr R, Mukherji D, Temraz S, Nassar F, et al. Ascorbic Acid in Colon Cancer: From the Basic to the Clinical Applications. Int J Mol Sci 2018;19(9):2752.
[180] Ngo YL, Lau CH, Chua LS. Review on rosmarinic acid extraction, fractionation and its anti-diabetic potential. Food Chem Toxicol 2018;121:687–700.
[181] da Silva SB, Amorim M, Fonte P, Madureira R, Ferreira D, Pintado M, et al. Natural extracts into chitosan nanocarriers for rosmarinic acid drug delivery. Pharm Biol 2015;53(5):642–52.
[182] Herizchi R, Abbasi E, Milani M, Akbarzadeh A. Current methods for synthesis of gold nanoparticles. Artif Cells, Nanomedicine, Biotechnol 2016;44(2):596–602.
[183] Allen JM, Xu J, Blahove M, Canonico-May SA, Santaloci TJ, Braselton ME, et al. Synthesis of less toxic gold nanorods by using dodecylethyldimethylammonium bromide as an alternative growth-directing surfactant. J Colloid Interface Sci 2017;505:1172–6.
[184] Bragta P, Sidhu RK, Jyoti K, Baldi A, Jain UK, Chandra R, et al. Intratumoral administration of carboplatin bearing poly (ε-caprolactone) nanoparticles amalgamated with in situ gel tendered augmented drug delivery, cytotoxicity, and apoptosis in melanoma tumor. Colloids Surfaces B Biointerfaces 2018;166:339–48.
[185] Holback H, Yeo Y. Intratumoral Drug Delivery with Nanoparticulate Carriers. Pharm Res 2011;28(8):1819–30.
[186] Öztürk AA, Yenilmez E, Özarda MG. Clarithromycin-Loaded Poly (Lactic-co-glycolic Acid) (PLGA) Nanoparticles for Oral Administration: Effect of Polymer Molecular Weight and Surface Modification with Chitosan on Formulation, Nanoparticle Characterization and Antibacterial Effects. Polymers (Basel) 2019;11(10):1632.
[187] Verma A, Stellacci F. Effect of Surface Properties on Nanoparticle-Cell Interactions. Small 2010;6(1):12–21.
[188] Robertson JD, Rizzello L, Avila-Olias M, Gaitzsch J, Contini C, Magoń MS, et al. Purification of Nanoparticles by Size and Shape. Sci Rep 2016;6(1):27494.
[189] Hwang N-M, Jung J-S, Lee D-K. Thermodynamics and Kinetics in the Synthesis of Monodisperse Nanoparticles. Thermodyn. - Fundam. Its Appl. Sci., InTech; 2012.
[190] Zhao J, Stenzel MH. Entry of nanoparticles into cells: the importance of nanoparticle properties. Polym Chem 2018;9(3):259–72.
[191] Hirn S, Semmler-Behnke M, Schleh C, Wenk A, Lipka J, Schäffler M, et al. Particle size-dependent and surface charge-dependent biodistribution of gold nanoparticles after intravenous administration. Eur J Pharm Biopharm 2011;77(3):407–16.

[192] Maciulevičius M, Vinčiūnas A, Brikas M, Butsen A, Tarasenka N, Tarasenko N, et al. Pulsed-laser generation of gold nanoparticles with on-line surface plasmon resonance detection. Appl Phys A 2013;111(1):289–95.
[193] ENSINGER C, SPIZZO G, MOSER P, TSCHOERNER I, PROMMEGGER R, GABRIEL M, et al. Epidermal Growth Factor Receptor as a Novel Therapeutic Target in Anaplastic Thyroid Carcinomas. Ann N Y Acad Sci 2004;1030(1):69–77.
[194] Magro G, Cataldo I, Amico P, Torrisi A, Vecchio GM, Parenti R, et al. Aberrant Expression of TfR1/CD71 in Thyroid Carcinomas Identifies a Novel Potential Diagnostic Marker and Therapeutic Target. Thyroid 2011;21(3):267–77.
[195] Campisi A, Bonfanti R, Raciti G, Bonaventura G, Legnani L, Magro G, et al. Gene Silencing of Transferrin-1 Receptor as a Potential Therapeutic Target for Human Follicular and Anaplastic Thyroid Cancer. Mol Ther - Oncolytics 2020;16:197–206.
[196] Liebner DA, Haraldsdottir S, Shah MH. Potential Approaches to Chemotherapy of Thyroid Cancer in the Future. Thyroid Cancer, New York, NY: Springer New York; 2016, p. 1001–6.
[197] Song C, Li F, Guo X, Chen W, Dong C, Zhang J, et al. Gold nanostars for cancer cell-targeted SERS-imaging and NIR light-triggered plasmonic photothermal therapy (PPTT) in the first and second biological windows. J Mater Chem B 2019;7(12):2001–8.
[198] ISO 10993-5:2009(E). Biological devices — Part 5: Tests for in vitro cytotoxicity n.d.;
[199] Amin K, Dannenfelser R-M. In vitro hemolysis: Guidance for the pharmaceutical scientist. J Pharm Sci 2006;95(6):1173–6.
[200] Gustafson HH, Holt-Casper D, Grainger DW, Ghandehari H. Nanoparticle uptake: The phagocyte problem. Nano Today 2015;10(4):487–510.
[201] De Jong WH, Hagens WI, Krystek P, Burger MC, Sips AJAM, Geertsma RE. Particle size-dependent organ distribution of gold nanoparticles after intravenous administration. Biomaterials 2008;29(12):1912–9.
[202] Sonavane G, Tomoda K, Makino K. Biodistribution of colloidal gold nanoparticles after intravenous administration: Effect of particle size. Colloids Surfaces B Biointerfaces 2008;66(2):274–80.
[203] Nave M, Castro RE, Rodrigues CM, Casini A, Soveral G, Gaspar MM. Nanoformulations of a potent copper-based aquaporin inhibitor with cytotoxic effect against cancer cells. Nanomedicine 2016;11(14):1817–30.
[204] Anderson GJ, Frazer DM. Hepatic Iron Metabolism. Semin Liver Dis 2005;25(04):420–32.
[205] Choi CHJ, Alabi CA, Webster P, Davis ME. Mechanism of active targeting in solid tumors with transferrin-containing gold nanoparticles. Proc Natl Acad Sci 2010;107(3):1235–40.
[206] Bartlett DW, Su H, Hildebrandt IJ, Weber WA, Davis ME. Impact of tumor-specific targeting on the biodistribution and efficacy of siRNA nanoparticles measured by multimodality in vivo imaging. Proc Natl Acad Sci 2007;104(39):15549–54.
[207] Li X, Hu Z, Ma J, Wang X, Zhang Y, Wang W, et al. The systematic evaluation of size-dependent toxicity and multi-time biodistribution of gold nanoparticles. Colloids Surfaces B Biointerfaces 2018;167:260–6.